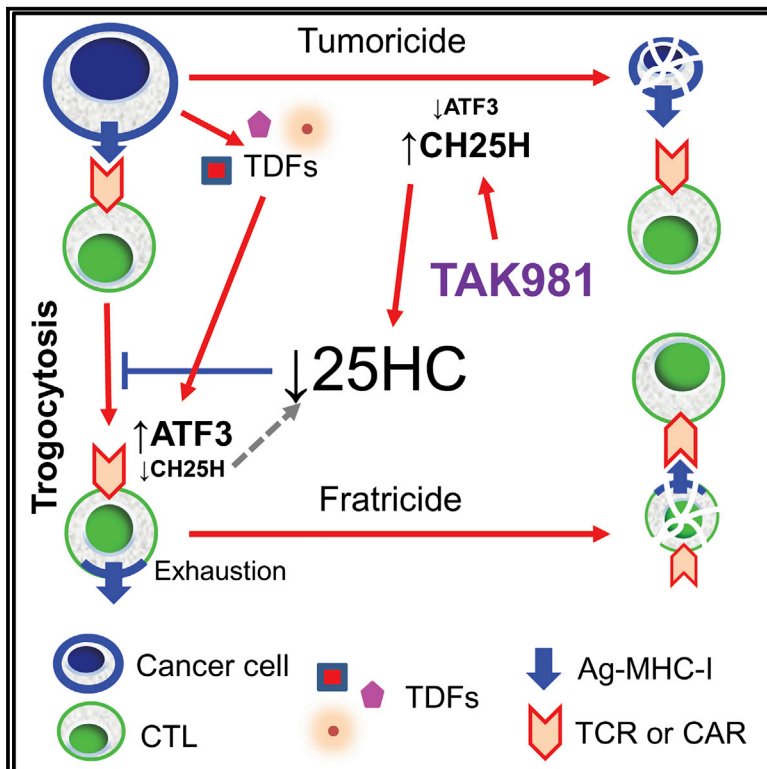


Cell Metabolism

ATF3 and CH25H regulate effector trogocytosis and anti-tumor activities of endogenous and immunotherapeutic cytotoxic T lymphocytes

Graphical abstract



Authors

Zhen Lu, Noreen McBrearty, Jinyun Chen, ..., J. Alan Diehl, Constantinos Koumenis, Serge Y. Fuchs

Correspondence

syfuchs@upenn.edu

In brief

Lu et al. demonstrate that partial loss of cholesterol 25-hydroxylase (CH25H) occurs in the intratumoral T cells. This loss leads to increased trogocytosis and suppresses viability and activity of native and therapeutic chimeric antigen receptor T cells. Boosting CH25H expression increases the efficacy of anti-tumor immunotherapy.

Highlights

- Tumor-derived factors stimulate effector trogocytosis and inhibit CAR T cells
- ATF3-driven downregulation of CH25H mediates trogocytosis and immunosuppression
- Loss of CH25H in endogenous cytotoxic T lymphocytes promotes tumor growth
- Co-expression of CH25H boosts the anti-tumor efficacy of therapeutic CAR T cells



Article

ATF3 and CH25H regulate effector trogocytosis and anti-tumor activities of endogenous and immunotherapeutic cytotoxic T lymphocytes

Zhen Lu,¹ Noreen McBrearty,¹ Jinyun Chen,¹ Vivek S. Tomar,¹ Hongru Zhang,¹ Gianluca De Rosa,¹ Aiwen Tan,² Aalim M. Weljie,² Daniel P. Beiting,³ Zhen Miao,⁴ Subin S. George,⁵ Allison Berger,⁶ Gurpanna Saggi,⁶ J. Alan Diehl,⁷ Constantinos Koumenis,⁸ and Serge Y. Fuchs^{1,9,*}

¹Department of Biomedical Sciences, University of Pennsylvania, Philadelphia, PA 19104, USA

²Department of Systems Pharmacology and Translational Therapeutics, University of Pennsylvania, Philadelphia, PA 19104, USA

³Department of Pathobiology, University of Pennsylvania, Philadelphia, PA 19104, USA

⁴Department of Genomics and Computational Biology, University of Pennsylvania, Philadelphia, PA 19104, USA

⁵Institute for Biomedical Informatics, University of Pennsylvania, Philadelphia, PA 19104, USA

⁶Takeda Development Center Americas, Inc., Lexington, MA 02421, USA

⁷Department of Biochemistry, Case Western Reserve University School of Medicine, Cleveland, OH 44106, USA

⁸Department of Radiation Oncology, University of Pennsylvania, Philadelphia, PA 19104, USA

⁹Lead contact

*Correspondence: syfuchs@upenn.edu

<https://doi.org/10.1016/j.cmet.2022.08.007>

SUMMARY

Effector trogocytosis between malignant cells and tumor-specific cytotoxic T lymphocytes (CTLs) contributes to immune evasion through antigen loss on target cells and fratricide of antigen-experienced CTLs by other CTLs. The mechanisms regulating these events in tumors remain poorly understood. Here, we demonstrate that tumor-derived factors (TDFs) stimulated effector trogocytosis and restricted CTLs' tumoricidal activity and viability *in vitro*. TDFs robustly altered the CTL's lipid profile, including depletion of 25-hydroxycholesterol (25HC). 25HC inhibited trogocytosis and prevented CTL's inactivation and fratricide. Mechanistically, TDFs induced ATF3 transcription factor that suppressed the expression of 25HC-regulating gene—cholesterol 25-hydroxylase (*CH25H*). Stimulation of trogocytosis in the intratumoral CTL by the ATF3-CH25H axis attenuated anti-tumor immunity, stimulated tumor growth, and impeded the efficacy of chimeric antigen receptor (CAR) T cell adoptive therapy. Through use of armored CAR constructs or pharmacologic agents restoring CH25H expression, we reversed these phenotypes and increased the efficacy of immunotherapies.

INTRODUCTION

Intercellular transfer of biomolecules contributes to organization of collective behavior of cells in a multi-cellular organism. This transfer can be mediated by a number of mechanisms including trogocytosis, which plays an important role in the regulation of immunity and other vital biological processes (Rechavi et al., 2009). Trogocytosis is an evolutionarily conserved process of extraction and subsequent transfer of fragments of cell membrane along with associated proteins and other biomolecules between cells that are in a close contact with each other. As a result of this transfer, a gain or loss of function for either acceptor or donor cells (or both) may occur (Dance, 2019; Rechavi et al., 2009).

The functional consequences of trogocytosis in T cells depend on the context and nature of partner cells. For example, in the course of antigen presentation, a priming T cell receptor-depen-

dent trogocytosis results in T cells to acquire membrane fragments along with the major histocompatibility complex (MHC) class I and class II proteins and co-stimulatory and other molecules from the antigen-presenting cells. The effector trogocytosis between activated CD8⁺ T cells (cytotoxic T lymphocytes [CTLs]) and target cells expressing specific antigen leads to a transfer of MHC-I-antigen complexes onto CTLs (reviewed in Ahmed et al. [2008]; Miyake and Karasuyama, 2021; Nakayama et al., 2021).

Intriguingly, effector trogocytosis between target malignant cells and therapeutic CD8⁺ T cells expressing the chimeric antigen receptor (CAR) is implicated in decreased clinical benefits of CTLs (Hamieh et al., 2019). Trogocytosis is associated with decreased viability and activity of chimeric antigen-expressing recipient CTLs due to their exhaustion, as well as killing by other CAR CTLs in a process called fratricide. Additionally, the loss of antigen on surviving donor malignant cells masks them from



subsequent attack by CAR T cells. These intricate and robust mechanisms help malignant cells to withstand CAR T cell adoptive therapies (Hamieh et al., 2019).

Tumors are adept at utilizing evolutionary conserved processes for evading the immune surveillance. However, it is not clear whether the described above mechanisms are also effective in naturally occurring anti-tumor CTLs. Furthermore, how effector trogocytosis is regulated and how this regulation can be altered during tumor growth is not well understood. Here, we present evidence for increased extent of trogocytosis in the tumor microenvironment. Our *in vitro* studies demonstrate that tumor-derived factors (TDFs) stimulate trogocytosis and decrease viability and activity of anti-tumor CTLs by reprogramming the regulatory axis that involves activating transcription factor-3 (ATF3) and cholesterol 25-hydroxylase (CH25H).

ATF3 is an early stress-responsive gene that could be induced by many factors of tumor microenvironment including hypoxia and nutrient deprivation (reviewed in Hai et al. [2010]). ATF3 has been shown to suppress CH25H expression in macrophages (Gold et al., 2012). Our results *in vitro* suggest that TDF-induced ATF3 in CTLs downregulates expression of CH25H. The latter catalyzes monooxygenation of cholesterol into 25-hydroxycholesterol (25HC) (Cyster et al., 2014), which interferes with trogocytosis stimulated by TDFs. Dysregulation of the ATF3-CH25H axis in the intratumoral natural or CAR-expressing CTLs stimulates effector trogocytosis and undermines viability and anti-tumor activity of these CTLs. Conversely, pharmacological or genetic restoration of CH25H expression in CTLs inhibits trogocytosis, suppresses tumor growth, and increases the efficacy of immunotherapies.

RESULTS

Tumor-derived factors downregulate 25HC and stimulate trogocytosis between effector CTL and malignant cells

Effector trogocytosis that transfers antigenic complexes to specific CTLs from malignant cells undermines their killing due to antigen loss and CTL fratricide (Hamieh et al., 2019). Mechanisms regulating the extent of effector trogocytosis are not well understood. We sought to determine how the factors present in the tumor microenvironment may affect the extent of trogocytosis (analyzed as in Figure S1A). To this end, CTLs were exposed to TDFs produced by MC38 colon adenocarcinoma cells and present within the tumor cell-conditioned media (TCM), as well as to purified factors such as prostaglandin E₂ (PGE₂) and vascular endothelial growth factor (VEGF), which are known to contribute to the immune suppressive properties of the tumor microenvironment (Rabinovich et al., 2007). As controls, we used analogous treatment with vehicle or media conditioned by mouse fibroblasts (FCM) or by intestinal epithelial cells (IECM).

We incubated pre-treated OT-I CTLs with ovalbumin (OVA)-expressing MC38 colon adenocarcinoma cells labeled with DiD lipophilic dye. We detected an increased transfer of DiD from MC38OVA cells onto co-incubated OT-I CTLs after their exposure to TCM, PGE₂, or VEGF (Figures 1A and S1B). This transfer was likely a result of trogocytosis, because it was notably inhibited by the loss of cell-cell contact due to separation of CTLs and MC38OVA cells in a Transwell setting (Figure S1C).

Furthermore, treatment of CTLs with inhibitor of actin polymerization Latrunculin A (previously shown to inhibit trogocytosis; Hamieh et al., 2019) or use of parental MC38 cells lacking OVA antigen notably inhibited DiD transfer onto CTLs (Figures S1C and S1D), indicating that this antigen-dependent transfer stimulated by the TDFs was a result of trogocytosis.

To delineate the mechanisms underlying TDF-dependent increase in effector trogocytosis, we profiled gene expression in CTLs treated with TCM. This treatment altered expression of genes involved in several key biological processes including the cholesterol metabolism pathway, which was notably suppressed (Figure 1B). Cholesterol controls many crucial properties of the lipid bilayers of biological membranes, such as their compressibility, fluidity, intrinsic curvature, and propensity for transfer and fusion (reviewed in Yang et al. [2016]). Given that these characteristics are instrumental for trogocytosis, we focused on this pathway.

Among the genes involved in cholesterol metabolism, *Ch25h* was the top downregulated gene (Figure S1E). Furthermore, expression of *Ch25h* was notably decreased among all genes affected by TCM (Figures 1C and 1D). We focused on CH25H because of its enzymatic role in production of 25HC (Cyster et al., 2014). 25HC is known to alter the fluidity of lipid membranes and to inhibit their fusion (Anggakusuma et al., 2015; Ortiz et al., 2019; Zang et al., 2020), which is essential for incorporating malignant cell membrane fragments into CTL during trogocytosis (Dance, 2019; Rechavi et al., 2009). Intriguingly, the lipidomics profiling of CTLs treated with TCM revealed numerous alterations in the content of specific lipid species (Figure 1E), such as a notable decrease in the levels of hydroxysterols including 25HC (Figures 1E and 1F).

Downregulation of *Ch25h* levels was seen in CTLs exposed to TDFs *in vitro* (Figure 1G). Accordingly, the intratumoral CTLs expressed less of *Ch25h* mRNA in comparison with the splenic CTLs (Figures 1H and 1I). Similar results were obtained in CTLs isolated from tumors and spleens in other syngeneic mouse tumor models including B16F10 melanoma, MH6499c4 pancreatic ductal adenocarcinoma, and Hepa1-6 hepatocellular carcinoma (Figure S1F). These results indicate that downregulation of CH25H in CTLs is induced by TDFs *in vitro* and occurs in the tumor microenvironment.

CH25H is a pivotal regulator of CTL trogocytosis, survival, and activity

We next determined the effects of 25HC on CTLs exposed to TDFs *in vitro*. Stimulation of trogocytosis (assessed by the transfer of OVA antigen complexed with MHC-I from MC38OVA cells onto OT-I CTLs) by TCM was inhibited by 25HC exposure (Figures S2A and 2A). Importantly, 25HC treatment abolished a decrease in viability elicited by TDFs in the antigen-experienced, but not antigen-naïve, CTL (Figure 2B). Furthermore, this treatment also reversed the suppressive effects of TDFs on ability of CTLs to kill MC38OVA target cells (Figure 2C), highlighting the importance of 25HC in the regulation of CTLs viability and function.

Considering that 25HC can directly inhibit fusion of lipid membranes (Anggakusuma et al., 2015; Ortiz et al., 2019; Zang et al., 2020), these effects may explain ability of 25HC to disrupt trogocytosis. However, additional mechanisms such as contribution of 25HC to the activation of the liver X receptor (LXR; as reviewed

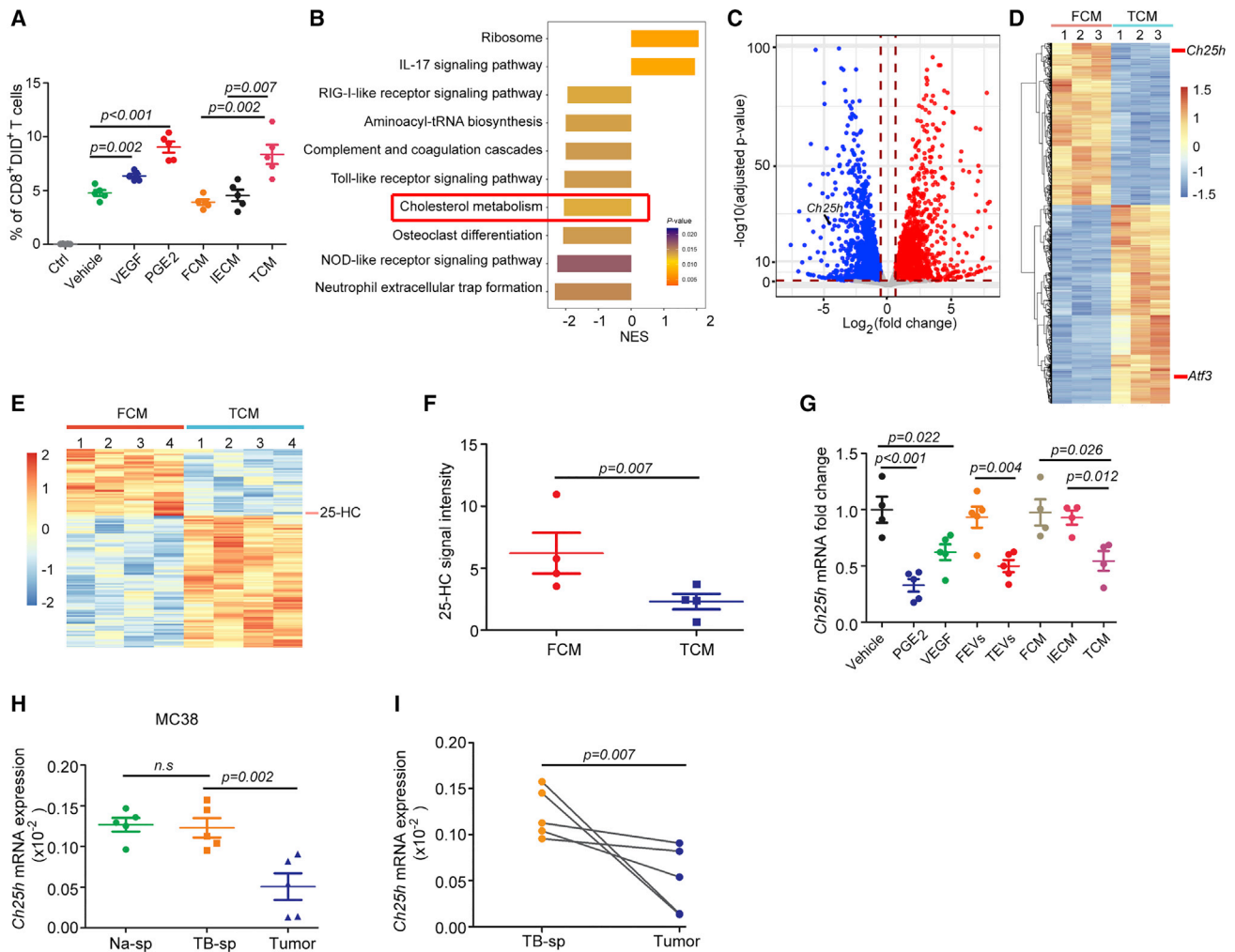


Figure 1. Tumor-derived factors downregulate 25-hydroxycholesterol and stimulate trogocytosis between effector CTL and malignant cells

(A) Analysis of transfer of DiD dye from DiD-labeled OVA-expressing MC38 cells onto co-cultured (for 4 h) OT-I CD8⁺ T cells pre-treated with VEGF (50 ng/ml), PGE₂ (10nM), FCM (fibroblast cell medium), IECM (intestinal epithelial cell medium), or TCM (tumor-conditioned medium) for 8 h as indicated (n = 5).

(B) KEGG enrichment analysis of altered pathways in CTLs treated with TCM (compared to FCM) for 8 h (n = 3).

(C) Volcano plot of differentially expressed genes in CTLs treated as in (B).

(D) Heatmap of differentially expressed genes in CTLs treated as in (B) (n = 3).

(E) Heatmap of changes in lipid species that occurred in CTLs treated as in (B) (n = 4).

(F) Levels of 25HC in CTLs treated as in (B) (n = 4).

(G) qPCR analysis of *Ch25h* mRNA expression in CTLs treated with vehicle; media conditioned by primary mouse intestinal epithelial cells (IECM), fibroblasts (FCM), or MC38 tumor cells (TCM); or PGE₂ (10nM), VEGF (50 ng/ml), or MC38 tumor-derived extracellular vesicles (TEVs; 20 μg/mL) for 8 h (n = 4 to 5).

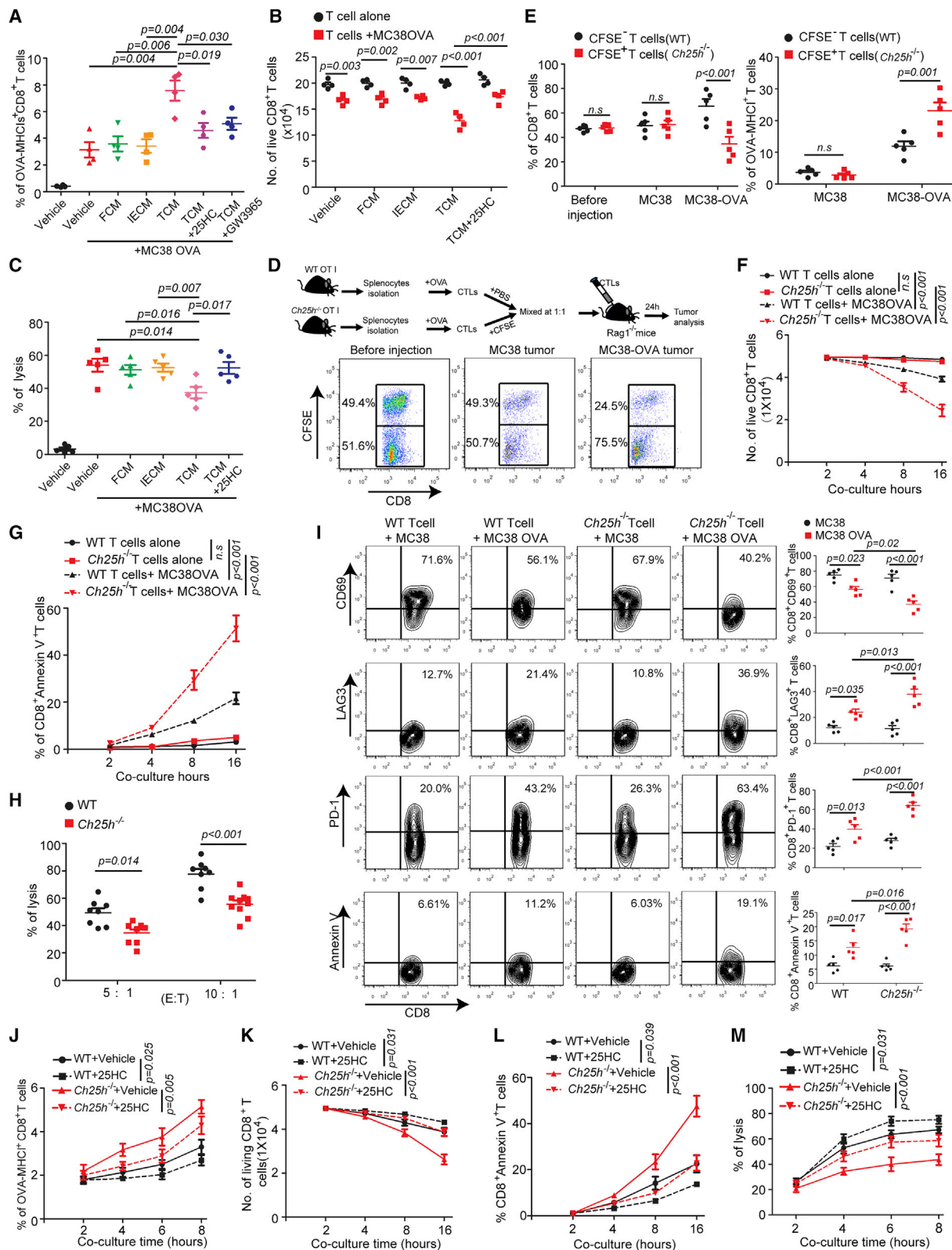
(H) qPCR analysis of *Ch25h* mRNA expression in CD8⁺ T cells isolated from MC38 tumors or spleens from naive or MC38 tumor-bearing mice (n = 5). Na-sp, spleen from naive mice; TB-sp, spleen from tumor-bearing mice.

(I) Pairwise comparison of *Ch25h* mRNA expression in CD8⁺ T cells isolated from tumor and spleen of individual mice (n = 5). Data are presented as mean ± SEM. Statistical analysis was performed using 2-tailed Student's t test. n.s., not significant.

See also Figure S1.

in Cyster et al. [2014]) cannot be ruled out. Indeed, treatment of TCM-exposed CD8⁺ T cells with 25HC upregulated known LXR-stimulated genes such as *Abca1*, *Abcg1*, *Lbp*, and *ApoE*. Similar results were obtained using a bona fide LXR agonist GW3965 (Figure S2B). Importantly, treatment with LXR agonist GW3965 inhibited the extent of trogocytosis (Figures 2A and S2A). These results demonstrate that 25HC in CTLs can contribute to activation of the LXR-dependent pathway and indirectly implicate LXR in the regulation of trogocytosis.

Given that CH25H is downregulated in the intratumoral CTLs (Figures 1H, 1I, and S1F), we sought to determine the importance of this regulation using cells from OT-I mice lacking *Ch25h* alleles. Knockout of this gene did not significantly affect activation (Figure S2C), proliferation (data not shown), exhaustion, or apoptosis (Figure S2D) of CD8⁺ T cells cultured alone. Thus, we assessed the extent of trogocytosis and CTL viability *in vivo*. To this end, we injected a mixture of selectively labeled wild-type (WT) and CH25H-deficient OT-I CTLs into either control MC38 or



(legend on next page)

antigen-bearing MC38OVA tumors grown in *Rag1*^{-/-} mice (Figures 2D and S2E). Whereas no difference was detected a day later in MC38 tumors, a notable decrease in numbers and increase in transfer of MHC-I-OVA was seen in *Ch25h*^{-/-} CTLs that were exposed to OVA antigen in MC38OVA tumors (Figures 2D and 2E). These results suggest that CH25H protects CTLs from trogocytosis and decrease in viability upon antigen exposure.

We next aimed to recapitulate these phenotypes *in vitro*. Indeed, knockout of *Ch25h* notably increased the ability of CTLs to undergo trogocytosis (Figure S2F). Pre-treatment of either WT or *Ch25h*-deficient cells with 25HC or LXR agonist GW3965 partially decreased the extent of trogocytosis (Figure S2F). This result indicates that LXR activated by 25HC might be involved in the regulation of trogocytosis but not does not rule out the LXR-independent effects of 25HC.

As expected, increased trogocytosis in *Ch25h*-null cells was antigen dependent and sensitive to Latrunculin A (Figures S2G–S2J). Moreover, when co-cultured with MC38OVA, the increased trogocytosis in *Ch25h*-deficient CTL was concomitant with decreased viability (Figure 2F), increased apoptosis (Figure 2G), and attenuated tumoricidal activity (Figure 2H). Furthermore, these cells displayed a reduced CD69 activation marker, increased LAG3 and PD-1 exhaustion markers, and increased apoptosis (Figure 2I). These results were further supported by experiments, in which adding 25HC to antigen-experienced CTLs reverted the effects of *Ch25h* ablation on the extent of trogocytosis (Figure 2J), viability (Figure 2K), apoptosis (Figure 2L), and tumoricidal activity (Figure 2M). Collectively, these results suggest that inactivation of CH25H in the tumor microenvironment stimulates trogocytosis and impedes viability and activity of the antigen-experienced CTLs.

Downregulation of CH25H in CTLs attenuates the immune responses and promote tumor growth

Because of downregulation of CH25H in the CTLs isolated from mouse tumors (Figures 1H and S1F) and decreased viability of

antigen-experienced CH25H-deficient CTLs (Figures 2F, 2G, 2K, and 2L), it is plausible that partial loss of CH25H in the tumor microenvironment may be linked with decrease in tumor-infiltrating lymphocytes. Thus, we next searched for a putative association between the intratumoral expression of *CH25H* and *CD8A*, a gene primarily expressed by tumor-infiltrating CTLs. Meta analysis of published data (Liu et al., 2020; Park et al., 2019) revealed a weak correlation between *CH25H* levels and tumor infiltration by CD8⁺ T cells and between expression of *CH25H* and *CD8A* in tumors from human patients with melanoma, colon, and pancreatic cancers (Figures S3A and S3B). Importantly, low levels of *CH25H* expression were correlated with poor prognosis manifested by decreased progression-free and overall survival in patients with melanoma (Figures 3A and 3B). In all, these results indirectly associate CH25H expression with infiltration of human tumors with CTLs and lesser progression of human cancers.

Driven by these data from human patients with cancer, we sought to determine the importance of expression of *CH25H* in CTLs for tumor growth. To this end, we crossed *Cd8a-Cre* and *Ch25h*^{fl/fl} mice to generate *Ch25h*^{ΔCD8} animals (Figure S3C). Whereas no major differences with WT mice was found in spleen or blood of these cells (Figures S3D and S3E), *Ch25h*^{ΔCD8} mice supported a notably accelerated growth of B16F10 melanoma tumors (Figures 3C and 3D). Similar results were obtained in other tumor types including MC38 (Figure S3F), MH6499c4 (Figure S3G), and Hepa1-6 (Figure S3H). Critically, tumors obtained from *Ch25h*^{ΔCD8} mice displayed reduced number and a lower frequency of tumor infiltrating CD8⁺ T cells (Figures 3E, 3F, S3I, and S3J). Of note, these CH25H-deficient intratumoral (but not splenic) CTLs expressed less CD69 (Figures 3G, S3I, and S3J) and more PD-1 (Figures 3H, S3I, and S3J) and exhibited a greater rate of apoptosis (Figures 3I, S3I, and S3J). These results indicate that the expression of CH25H in the intratumoral CTLs plays an important role in their activity and viability. Conversely, inactivation of CH25H in CTLs attenuates the anti-tumor immune responses and promotes tumor growth.

Figure 2. CH25H is a pivotal regulator of CTL trogocytosis, survival, and activity

- (A) Analysis of transfer of OVA-MHC-I complexes from OVA-expressing MC38 cells onto co-cultured (for 4 h) OT-I CD8⁺ T cells pre-treated with FCM or IECM or TCM (with or without 25HC [4μM] or GW3965 [2μM]) for 8 h (n = 4).
- (B) Number of live CD8⁺ CTLs after co-culture experiment described in (A) (n = 4).
- (C) Luciferase activity-based analysis of lysis of MC38OVA-luc cells incubated with OT-I CD8⁺ T cells pre-treated with FCM or IECM or TCM (with or without 25HC, 4μM) for 8 h (n = 5).
- (D) A schematic of experiment for assessing the role of *Ch25h* in viability of CD8⁺ T cells *in vivo* (upper panel). Lower panel depicts the flow cytometry analysis of the percentage of CFSE⁺ CD8⁺ or CFSE⁻ CD8⁺ T cells isolated from the MC38 or MC38-OVA tumors 24 h after inoculation.
- (E) Quantification of viable CFSE⁺ or CFSE⁻ CD8⁺ T cells (left) and of transfer of OVA-MHC-I complexes on indicated CTLs (right) from experiment described in (D) (n = 5).
- (F) Analysis of number of live WT or *Ch25h*^{-/-} OT-I CD8⁺ T cells cultured alone or with MC38OVA target cells for indicated time (n = 3–5).
- (G) Analysis of percentage of apoptotic (annexin V+) T cells treated as in (F) (n = 3–5).
- (H) Luciferase-based analysis of lysis of MC38OVA-luc cells incubated with WT or CH25H-null OT-I CD8⁺ T cells at indicated E:T ratios for 4 h (n = 8–10).
- (I) Flow cytometry analysis of expression of indicated markers on the surface of WT or CH25H-null CD8⁺ OT-I T cells after co-culture with MC38OVA target cells or MC38 cells (as an antigen-lacking control) for 8 h (n = 5).
- (J) Quantification of transfer of OVA-MHC-I complexes from MC38OVA target cells on WT or CH25H-null CD8⁺ OT-I T cells pre-treated or not with 25HC (4μM for 8 h) (n = 5).
- (K) Numbers of live CTLs from experiment described in (J) (n = 5).
- (L) Percentage of apoptotic CTLs from experiment described in (J) (n = 5).
- (M) Luciferase-based analysis of lysis of MC38OVA-luc cells incubated with WT or CH25H-null OT-I CD8⁺ T cells pre-treated or not with 25HC (4μM for 8h) (n = 5). Data are presented as mean ± SEM. Statistical analysis was performed using 2-tailed Student's t test (A and C) or 1-way ANOVA with Tukey's multiple-comparison test (B, E, F, G, H, I, J, K, L, and M). n.s., not significant. See also Figure S2.

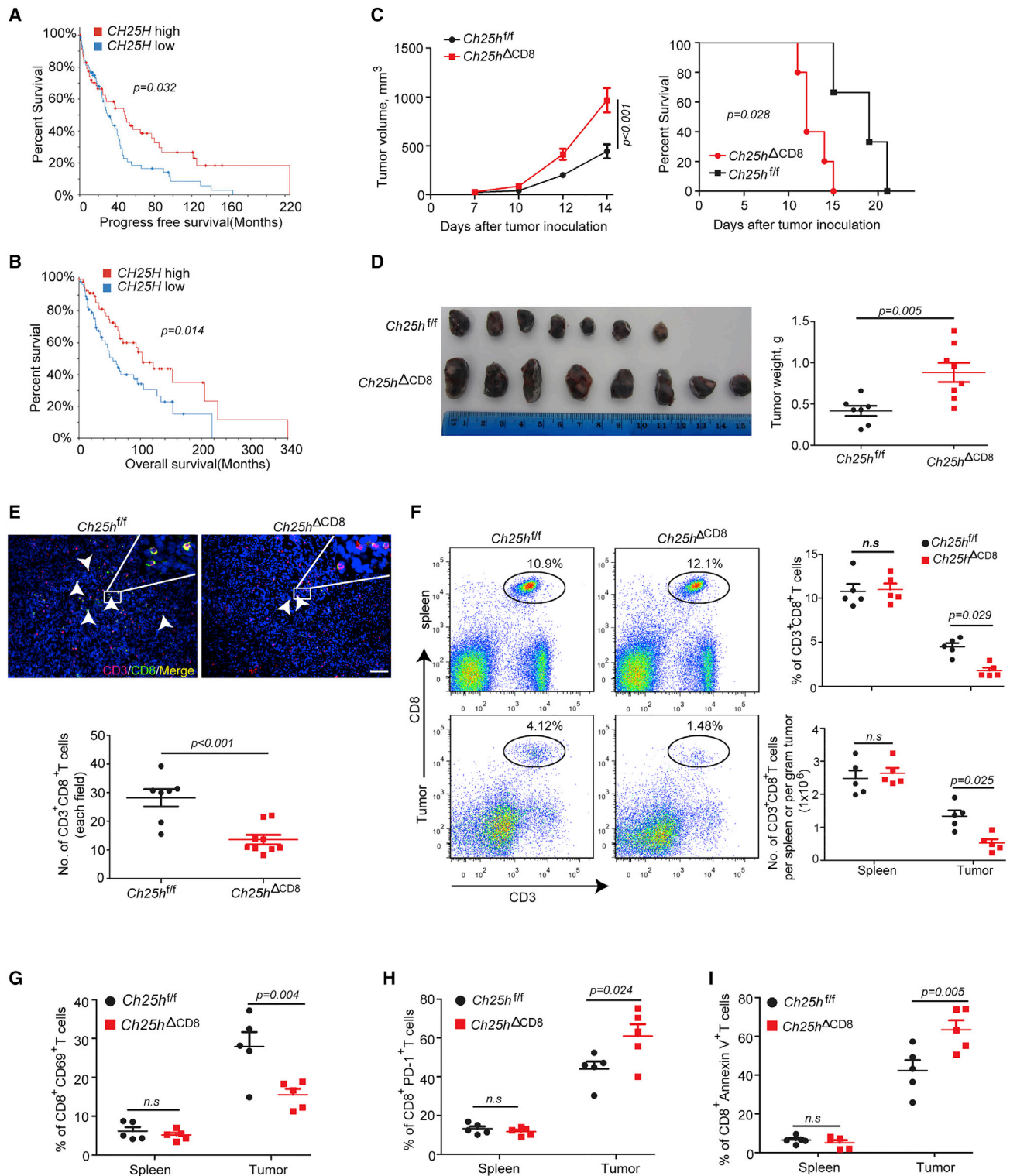


Figure 3. Downregulation of CH25H in CTLs attenuates the immune responses and promote tumor growth

(A) Association between CH25H expression and progress free survival in human melanoma patients.

(B) Association between CH25H expression and overall survival in human melanoma patients.

(C) Growth of B16F10 melanoma tumors (inoculated s.c. at 1×10^6) in *Ch25h^{fl/fl}* and *Ch25h^{ΔCD8}* mice (left; n = 9 to 10) and survival analysis for tumor-bearing animals (right; n = 7 to 8).

(D) Representative images of B16F10 tumor size (left) and weight (right) at day 15 from experiment described in (C).

(legend continued on next page)

ATF3 regulates effector trogocytosis, activity, and viability of CTLs and tumor growth in a CH25H-dependent manner

We next sought to delineate the mechanisms underlying downregulation of CH25H in the intratumoral CTLs. ATF3 is a key negative regulator of CH25H expression in macrophages (Gold et al., 2012; Labzin et al., 2015). Chromatin immunoprecipitation assay demonstrated that ATF3 was present on the promoter of the *Ch25h* gene in mouse OT-I CD8⁺ T cells and treatment of these cells with TDFs increased this binding (Figure 4A). Importantly, ATF3 is well known as an early stress-responsive gene that could be induced by many factors of tumor microenvironment (reviewed in Hai et al. [2010]). We noted an induction of ATF3 in CTLs treated with media conditioned by MC38 colon adenocarcinoma cells, but not by normal intestinal cells or fibroblasts (Figures 1D and S4A). Furthermore, specific TDFs such as PGE₂, VEGF, and tumor-derived extracellular vesicles were all capable of increasing *Atf3* expression in CD8⁺ T cells *in vitro* (Figure S4A).

Likewise, analysis of CD8⁺ T cells isolated from MC38 tumors revealed an increase in ATF3 mRNA and protein levels compared to such cells from spleens of either tumor-bearing or naive mice (Figures 4B and 4C). *ATF3* induction was also noted in the intratumoral CTLs from B16F10, MH6499c4, and Hepa1-6 tumors (Figure S4B). Importantly, in these models, the expression of *Atf3* in the intratumoral CTLs often negatively correlated with *Ch25h* levels (Figures 4D and S4C). These results are consistent with a hypothesis wherein ATF3 induced in the intratumoral CTLs by TDFs plays an important role in downregulation of CH25H.

To definitively test this possibility, we have generated *Atf3*^{ΔCD8} mice, which lacked ATF3 in CD8⁺ cells but did not differ from *Atf3*^{fl/fl} controls in the composition of immune cells in spleen or blood (Figure S4D). Nevertheless, CTL from *Atf3*^{ΔCD8} mice did not downregulate CH25H in response to *in vitro* treatment with TDFs (Figure 4E). Importantly, downregulation of CH25H in the CTLs isolated from MC38 tumors was less pronounced when these tumors grew in *Atf3*^{ΔCD8} mice (Figure 4F). Similar results were obtained in other tumor types (Figure S4E), suggesting that ATF3 contributes to decreased expression of CH25H in the intratumoral CTLs.

Examination of tumor volumes from these experiments revealed a significantly slower growth of MC38 tumors in *Atf3*^{ΔCD8} mice compared to *Atf3*^{fl/fl} controls (Figure 4G). Furthermore, genetic ablation of ATF3 in CTLs increased frequency of these cells within tumors (Figure 4H) and decreased expression of markers of exhaustion and apoptosis on these cells in the tumor microenvironment (Figure S4F). Similar results were found in CTL from B16F10 tumors (Figure 4I, 4J, and S4G–S4I), but not from spleens of B16F10-bearing mice (Figure S4J). Importantly, all

phenotypes associated with ablation of *Atf3* in CD8⁺ T cells were reversed upon concurrent ablation of *Ch25h* (Figures 4I, 4J, and S4G–S4I). These results indicate that ATF3-driven downregulation of CH25H in the intratumoral CTLs decreases their viability, suppresses the anti-tumor immune responses, and stimulates tumor growth.

ATF3 and CH25H control trogocytosis and activity of CAR T cells

To directly examine the role of the ATF3–Ch25h regulatory axis in effector trogocytosis as well as viability and function of CTLs, we generated WT, *Ch25h*^{ΔCD8}, *Atf3*^{ΔCD8}, and *Ch25h;Atf3*^{ΔCD8} murine T cells stably transduced with retrovirus for expression of CAR that target human CD19 (hCD19; Figure S5A). Upon incubation with target B16F10-hCD19 cells, we observed trogocytosis manifested by a transfer of hCD19 onto CAR T cells. Similar to results obtained in the OVA-OT-I model (Figure 2), knockout of CH25H stimulated trogocytosis (Figure 5A). Furthermore, under these conditions, CAR T cells lacking CH25H exhibited greater signs of exhaustion (Figure 5B) and apoptosis (Figure 5C) and were less effective in lysis of target B16F10-hCD19 cells (Figure 5D). Importantly, effector trogocytosis was inhibited in ATF3-deficient CAR T cells, whereas these cells were less exhausted and less apoptotic (Figures 5B and 5C) and more effective in killing antigen-expressing malignant cells (Figure 5D). Importantly, all these phenotypes associated with ATF3 deletion were largely reverted by genetic ablation of CH25H (Figures 5A–5D).

These results suggest a critical role for the ATF3–CH25H axis in the regulation of the extent of trogocytosis, viability, and activity of CAR T cells *in vitro*. We further corroborated these results by adoptive transfer of CAR WT, *Ch25h*^{ΔCD8}, *Atf3*^{ΔCD8}, or *Ch25h;Atf3*^{ΔCD8} T cells into *Rag1*^{−/−} mice bearing B16F10-hCD19 tumors. We then isolated CAR T cells from tumors and analyzed their status. A greater extent of trogocytosis (manifested by frequency of hCD19+ CD8⁺ T cells) and increase in exhaustion markers were noted in CH25H-null CAR T cells (Figures 5E, 5F, S5B, and S5C). Whereas the opposite trends were seen in the intratumoral *Atf3*^{ΔCD8} CAR T cells, the effects of ATF3 deletion were abolished by additional knockout of CH25H (Figures 5E, 5F, S5B, and S5C) suggesting an important role for ATF3–CH25H in regulating CAR T viability and activity *in vivo*.

Indeed, evaluation of TILs in these B16F10-hCD19 tumors revealed a greater infiltration of tumors by ATF3-deficient CAR T cells, whereas knockout of CH25H decreased the numbers and frequencies of intratumoral CTLs regardless of the status of ATF3 (Figure 5G). Accordingly, CAR T cells from *Atf3*^{ΔCD8} mice exhibited a greater anti-tumor activity as manifested by changes in tumor volume and weight (Figure 5H) and animal survival (Figure 5I). Importantly, knockout of CH25H attenuated the

(E) Immunofluorescence analysis and its quantification for numbers of CD3⁺CD8⁺ T cells in MC38 tumors from *Ch25h*^{fl/fl} and *Ch25h*^{ΔCD8}Cre mice (n = 7–9). Scale bar: 100 μm.

(F) Flow cytometry analysis of numbers and percentage of CD3⁺CD8⁺ T cells in MC38 tumors and spleens from tumor-bearing *Ch25h*^{fl/fl} and *Ch25h*^{ΔCD8}Cre mice (n = 5).

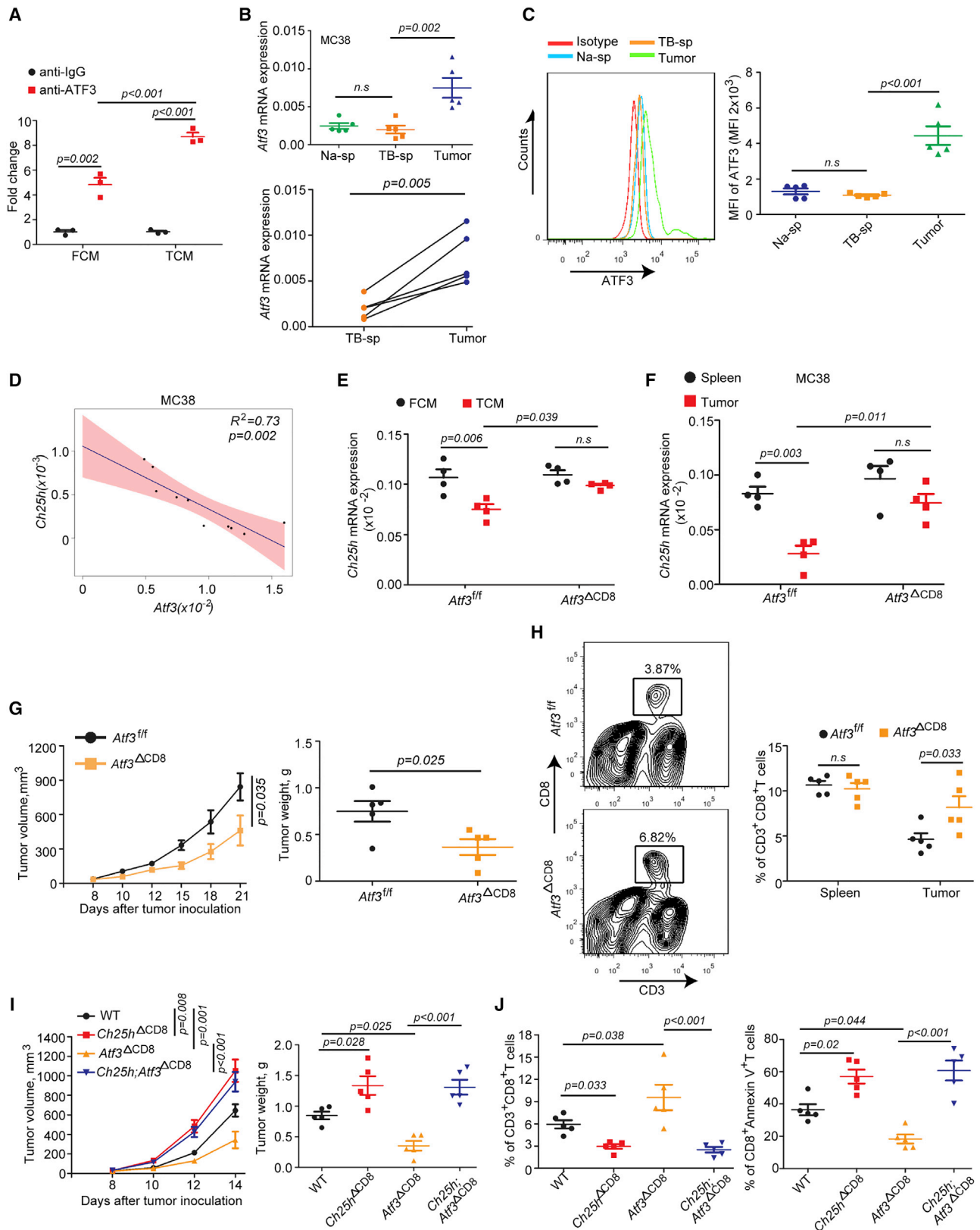
(G) Flow cytometry analysis of percentage of CD69-expressing CTLs from experiment described in (F).

(H) Flow cytometry analysis of percentage of PD-1-expressing CTLs from experiment described in (F).

(I) Flow cytometry analysis of percentage of Annexin V-expressing CTLs from experiment described in (F).

Data are presented as mean ± SEM. Statistical analysis was performed using 2-tailed Student's t test (D and E) or 1-way ANOVA with Tukey's multiple-comparison test (F, G, H, and I) or 2-way ANOVA with Sidak's multiple-comparison test (C) or log-rank (Mantel-Cox) test (A, B, and C). n.s., not significant.

See also Figure S3.



(legend on next page)

efficacy of CAR T cell therapy in any genetic context tested here (Figures 5H and 5I). These results characterize the ATF3-CH25H axis as a pivotal regulator of effector trogocytosis and associated changes in CAR T cell viability and efficacy of their anti-tumor effects.

TAK981 sumoylation inhibitor upregulates CH25H, inhibits trogocytosis, and augments CAR T cells viability and anti-tumor activities

We next sought a pharmacologic approach to suppressing the effector trogocytosis in order to increase viability and activity of the intratumoral CTLs. Although 25HC worked well *in vitro* (Figure 2), its suboptimal bioavailability (Li et al., 2017) prompted us to search for a medically relevant small molecule agent that could interfere with ATF3-driven downregulation of CH25H and restore CH25H levels in the intratumoral CTLs. After extensive analysis of literature, we chose to use an inhibitor of the sumoylation pathway because of the following factors: (1) ATF3 directly suppresses transcription of *CH25H* (Gold et al., 2012), and transcriptional repression is often associated with protein sumoylation (Lyst and Stancheva, 2007); (2) de-sumoylation of some transcriptional regulators is required for induction of ATF3 (Barysch et al., 2021); (3) importantly, sumoylation of ATF3 itself has been implicated in its transcriptional suppressive activities (Wang et al., 2013); and (4) in addition, activation of innate and adaptive immunity was observed upon genetic (Decque et al., 2016) or pharmacologic (Lightcap et al., 2021) disruption of the sumoylation pathway.

Intriguingly, exposure of activated OT-I CD8⁺ T cells with TDFs increased the levels of both unmodified and sumoylated ATF3 (Figure S6A). We then tested the ability of selective and potent sumoylation inhibitor TAK981 (Lightcap et al., 2021) to restore the CH25H expression in TDFs-exposed CTLs. Pre-treatment of TDFs-treated CD8⁺ T cells with TAK981 *in vitro* partially attenuated the increase in ATF3 mRNA expression and in levels of sumoylated and unmodified ATF3 protein (Figures S6A and S6B). Furthermore, TAK981 robustly prevented downregulation of CH25H (Figure 6A). We noted that, while TDFs stimulated trogocytosis (assessed by a transfer of the MHC-I-OVA complexes from MC38OVA target tumor cells onto OT-I CTLs), adding TAK981 prevented this stimulation. Importantly, this effect of TAK981 was seen in WT OT-I, but not in *Ch25h*^{-/-} OT-I, cells (Figure 6B) indicating that this sumoylation inhibitor can suppress trogocytosis by maintaining the levels of CH25H.

Given that effector trogocytosis of CTLs has been associated with decreased viability and functionality, we examined the effects of TAK981 along with TDFs on these parameters. These treatments did not affect numbers of OT-I CTLs, which were not exposed to OVA antigen. However, we noted a decrease in the numbers of WT OT-I CTLs upon their incubation with TCM in the presence of target MC38OVA tumor cells (Figure S6C). Under these conditions, treatment with TAK981 restored the numbers of WT OT-I cells in the culture. Importantly, compared to WT cells, the numbers of co-cultured CH25H-deficient OT-I CTLs were notably lower, and they did not increase in response to TAK981 treatment (Figure S6C). Likewise, TAK981 restored the tumoricidal activity of WT (but not *Ch25h*-null) OT-I CTLs against target MC38OVA tumor cells otherwise suppressed by TCM (Figure S6D). These results further suggest that TAK981 prevents trogocytosis and associated decrease in viability and activity of CTLs in a CH25H-dependent manner.

Whereas monotherapy of MC38 tumors in WT mice with TAK981 elicited a modest therapeutic effect, the combination of this agent with anti-PD1 checkpoint inhibitor notably suppressed tumor growth (Lightcap et al., 2021). In *Ch25h*^{fl/fl} mice under the same conditions, treatment with TAK981 alone or combined with anti-PD1 increased expression of CD69 and decreased levels of PD-1 and annexin-V on the intratumoral CTLs (Figures 6C and 6D). We also observed that TAK981+anti-PD1 combination significantly decreased tumor volume and weight and prolonged animal survival (Figures 6E–6G). Importantly, analysis of intratumoral CD8⁺ T cells reveal that TAK981 treatment downregulated ATF3 and upregulated CH25H *in vivo* (Figure S6E). Furthermore, consistent with ability of TAK981 to inhibit trogocytosis (Figure 6A) and apoptosis (Figure 6D), inclusion of this agent into therapeutic regimens also increased infiltration of MC38 tumors with CTLs (Figure S6F). Importantly, these effects were limited to the intratumoral CTLs and were not observed in the spleens from the same animals (Figure S6G).

Given that protein sumoylation affects numerous biologically important processes (Geiss-Friedlander and Melchior, 2007), these phenotypes cannot be attributed entirely to the effects of TAK981 on the levels of CH25H and on the extent of effector trogocytosis. However, ablation of CH25H in CD8⁺ T cells rendered these cells and their host mice much less sensitive to effects of TAK981, anti-PD1, and their combination (Figures 6C–6G). These results are consistent with our hypothesis that, albeit not essential, the prevention of CH25H downregulation in the

Figure 4. ATF3 regulates effector trogocytosis, activity, and viability of CTLs and tumor growth in a CH25H-dependent manner

- (A) ChIP-qPCR analysis of ATF3 binding to *Ch25h* promoter in OT-I CD8⁺ T cells treated or not with MC38 TCM for 12 h (n = 3).
 (B) Overall (upper) and pairwise (below) qPCR analysis of *Atf3* mRNA levels in CD8⁺ T cells from MC38 tumor tissue and spleen of naive or tumor-bearing mice (n = 5).
 (C) Flow cytometry analysis of ATF3 protein level in CD8⁺ T cells from MC38 tumor tissue and spleen of naive or tumor-bearing mice (n = 5).
 (D) Linear regression analysis of *Atf3* and *Ch25h* mRNA expression in CD8⁺ T cells isolated from MC38 tumors (n = 10).
 (E) Analysis of *Ch25h* expression in *Atf3*^{fl/fl} or *Atf3*^{ΔCD8} CD8⁺ T cells treated *in vitro* with TCM or FCM for 8 h (n = 5).
 (F) Analysis of *Ch25h* expression in CD8⁺ T cells isolated from MC38 tumor that grew in *Atf3*^{fl/fl} or *Atf3*^{ΔCD8} mice (n = 5).
 (G) Volume and weight of MC38 s.c. tumors that grew in *Atf3*^{fl/fl} or *Atf3*^{ΔCD8} mice (n = 5).
 (H) Flow cytometry assay of percentage of CD3⁺CD8⁺ T cells in MC38 tumors from *Atf3*^{fl/fl} or *Atf3*^{ΔCD8} mice (n = 5).
 (I) Volume and weight of B16F10 tumors that grew in WT, *Ch25h*^{ΔCD8}, *Atf3*^{ΔCD8}, or *Ch25h;Atf3*^{ΔCD8} mice (n = 5).
 (J) Percentage of CD3⁺CD8⁺ T cells and annexin V-positive CD3⁺CD8⁺ T cells from experiment described in (I) (n = 5).

Data are presented as mean ± SEM. Statistical analysis was performed using 2-tailed Student's t test (B, C, and G), linear regression analysis (D), 1-way ANOVA with Tukey's multiple-comparison test (A, E, F, H, I, and J) or 2-way ANOVA with Sidak's multiple-comparison test (G and I). n.s., not significant. See also Figure S4.

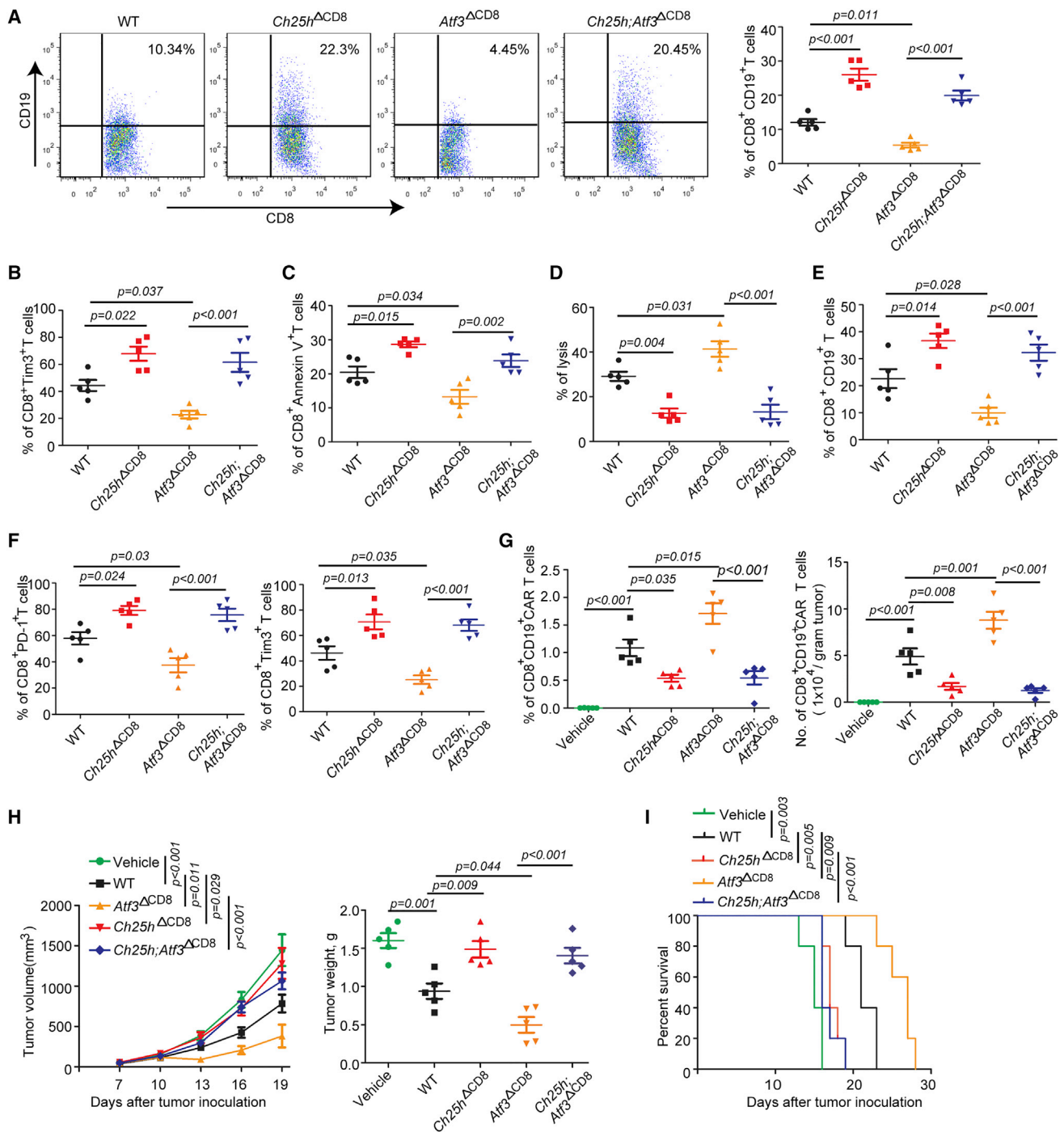


Figure 5. ATF3 and CH25H control trogocytosis and activity of CAR T cells

(A) Flow cytometry analysis of transfer of CD19 from B16F10-hCD19 target cells onto anti-CD19 CAR T cells (co-incubated for 4 h) produced from WT, $Ch25h^{\Delta CD8}$, $Atf3^{\Delta CD8}$, or $Atf3;Ch25h^{\Delta CD8}$ splenic T cells (n = 5).

(B) Flow cytometry analysis of the percentage of CD8⁺Tim3⁺ anti-CD19-CAR T cells processed as in (A) (n = 5).

(C) Flow cytometry analysis of the percentage of CD8⁺Annexin V⁺ anti-CD19-CAR T cells processed as in (A) (n = 5).

(D) Luciferase-based analysis of lysis of B16F10-hCD19-luc cells incubated with indicated anti-CD19 CAR T cells *in vitro* (n = 5).

(E) Percentage of CD19⁺ CD8⁺ T cells isolated from B16F10-hCD19 tumors that grew in $Rag1^{-/-}$ mice treated with WT, $Ch25h^{\Delta CD8}$, $Atf3^{\Delta CD8}$, or $Ch25h;Atf3^{\Delta CD8}$ anti-CD19 CAR T cells (n = 5).

(F) Percentage of CD8⁺PD-1⁺ T cells and CD8⁺Tim3⁺ T cells isolated from B16F10-hCD19 tumors treated as in (E) (n = 5).

(G) Percentage and absolute number of CD8⁺ anti-CD19 CAR⁺ T cells infiltrated into B16F10-hCD19 tumors treated as in (E) (n = 5).

(H) Volume and weight of B16F10-hCD19 tumor that grew in $Rag1^{-/-}$ mice treated with indicated anti-CD19 CAR T cells (n = 5).

(legend continued on next page)

intratumoral CTLs represents an important mechanism of action for anti-cancer therapies that involve TAK981.

Armored CAR designed to re-express CH25H inhibit trogocytosis and increase therapeutic efficacy

To counteract downregulation of CH25H in the intratumoral CTLs, we re-designed previously described anti-MESO and anti-CD19 CARs (Milone et al., 2009) to enable the co-expression of CH25H (Figure 7A). The ability of mouse CTLs expressing conventional anti-MESO CART to kill target EM-Meso-GFP-Luc cells (Figure S7A) was notably attenuated by knockout of CH25H but was restored with treatment with 25HC *in vitro* (Figure S7B). Experiments comparing CTLs harboring either conventional CAR or CAR armored with CH25H (Figure S7C) revealed that re-expression of CH25H notably inhibited the extent of trogocytosis (Figure 7B) and increased viability (Figure 7C) and tumoricidal activity (Figure 7D) of CAR T cells. Accordingly, treatment of NSG mice harboring EM-Meso-GFP-Luc tumors (Figure 7E) with CTLs harboring conventional or CH25H-expressing anti-MESO CAR revealed that expression of CH25H significantly increased the efficacy of this adoptive cell therapy as seen from assessment of tumor volume and weight and animal survival (Figures 7F and S7D). Under these conditions, T cells harboring CH25H-expressing armored CAR displayed increased numbers in tumors and blood compared to control CART T cells (Figures 7G and S7E).

To corroborate these data, we used another set of CARs designed against hCD19 (Figures 7A, S7F, and S7G). When tested *in vitro*, CAR T cells that co-express CH25H exhibited a greater killing activity (Figure S7H), and decreased trogocytosis manifested by transfer of antigen onto CTLs (Figure S7I) or by disappearance of antigen from target tumor cells (Figure S7J). CH25H-expressing CAR T cells also displayed lesser exhaustion (Figure S7K), and improved viability (Figure S7L). Furthermore, when tested *in vivo*, CAR T cells expressing CH25H demonstrated a greater therapeutic efficacy against B16F10-hCD19 tumors (Figure 7H and S7M), better infiltrated these tumors (Figure S7N), and expressed lower levels of markers of exhaustion and apoptosis (Figure S7O).

We next tested the effects of co-expressing CH25H on the efficacy of adoptive transfer of human CAR T cells harboring anti-CD19 CAR in the model of NALM6 acute B cell leukemia (Figure 7I). Under these conditions, CAR T cells expressing CH25H better persisted in the host (Figure 7J) and exhibited a greater anti-tumor efficacy as manifested by decreased number of leukemic cells in the blood (Figure 7K) and prolonged animal survival (Figure 7L). Collectively, these data argue that re-expression of CH25H in adoptively transferred CAR T cells protects them from trogocytosis and associated exhaustion and death and increases their tumoricidal activity and therapeutic potential.

DISCUSSION

Data presented herein reveal that activation of ATF3 and ensuing suppression of CH25H in the tumor microenvironment stimulate

the extent of effector trogocytosis between tumor-specific CTLs and malignant cells. These events also limit viability and activity of the intratumoral CTLs thereby stimulating tumor growth and eliciting resistance against adoptive cell transfer therapies including CAR T cell-based regimens. Maintaining expression of CH25H by administration of TAK981 sumoylation inhibitor or co-expressing CH25H along with CAR leads to restricted trogocytosis, increased survival and activity of CTLs, and improved efficacy of CAR T cell treatment. It is, however, important to note that TDFs elicited diverse and numerous changes in CTLs' gene expression profile as well as distinct alterations in levels of lipid species (Figure 1). Given that ATF3 is an early stress-responsive gene that could be induced by many factors of tumor microenvironment (Hai et al., 2010), it is plausible that many redundant factors besides PGE₂ and VEGF are capable of downregulating CH25H and promoting trogocytosis. Furthermore, although our data clearly implicate the ATF3-CH25H regulatory axis in TDFs-stimulated trogocytosis, we should not rule out additional potentially important mechanisms by which trogocytosis can be upregulated in the tumor microenvironment.

Results of studies utilizing TAK981 suggest that protein sumoylation may contribute to both induction of ATF3 and ATF3-dependent suppression of CH25H. Although sumoylation can occur on ATF3 itself (Wang et al., 2013), it is very likely that disrupted sumoylation of other important regulators contributes to ability of TAK981 to restore CH25H expression and inhibit trogocytosis. Additional studies are warranted to unravel these potentially interesting and important mechanisms that may lead to identification of additional targets and pharmacologic agents that could counteract trogocytosis associated with downregulation of CH25H in CTLs.

Our data further suggest a mechanism by which CH25H inhibits trogocytosis. Although inactivation of CH25H can channel cholesterol monoxygenation toward formation of other biologically and immunologically active oxysterols (such as 27-hydroxycholesterol (Baek et al., 2017)), we think that negative regulation of trogocytosis by CH25H is conferred by production of 25HC. Indeed, we observed a decrease in 25HC in CTLs exposed to the TDFs (Figure 1). Furthermore, current studies demonstrate a direct inhibitory effect of 25HC on trogocytosis and associated defects in viability and activity of CTLs (Figure 2). Furthermore, 25HC is known to inhibit lipid membrane fusion (Anggakusuma et al., 2015; Zang et al., 2020), which must happen for incorporating malignant cell membrane fragments into CTL during trogocytosis. These activities of 25HC are also implicated in suppression of uptake of the tumor-derived extracellular vesicles (Lu et al., 2021; Ortiz et al., 2019), which were proposed to contribute to the process of transfer of T cell receptor-containing complexes (Choudhuri et al., 2014). Importantly, 25-hydroxylation along with other modifications generates ligands for the LXR pathway (Cyster et al., 2014). Inhibition of trogocytosis in T cells treated with LXR agonist is suggestive of a role for the LXR pathway—potentially downstream of the

(I) Survival analysis for mice described in (H) (n = 5).

Data are presented as mean ± SEM. Statistical analysis was performed using 1-way ANOVA with Tukey's multiple-comparison test (A, B, C, D, E, F, G, and H) or 2-way ANOVA with Sidak's multiple-comparison test (H) or Kaplan-Meier test (I). n.s., not significant. See also Figure S5.

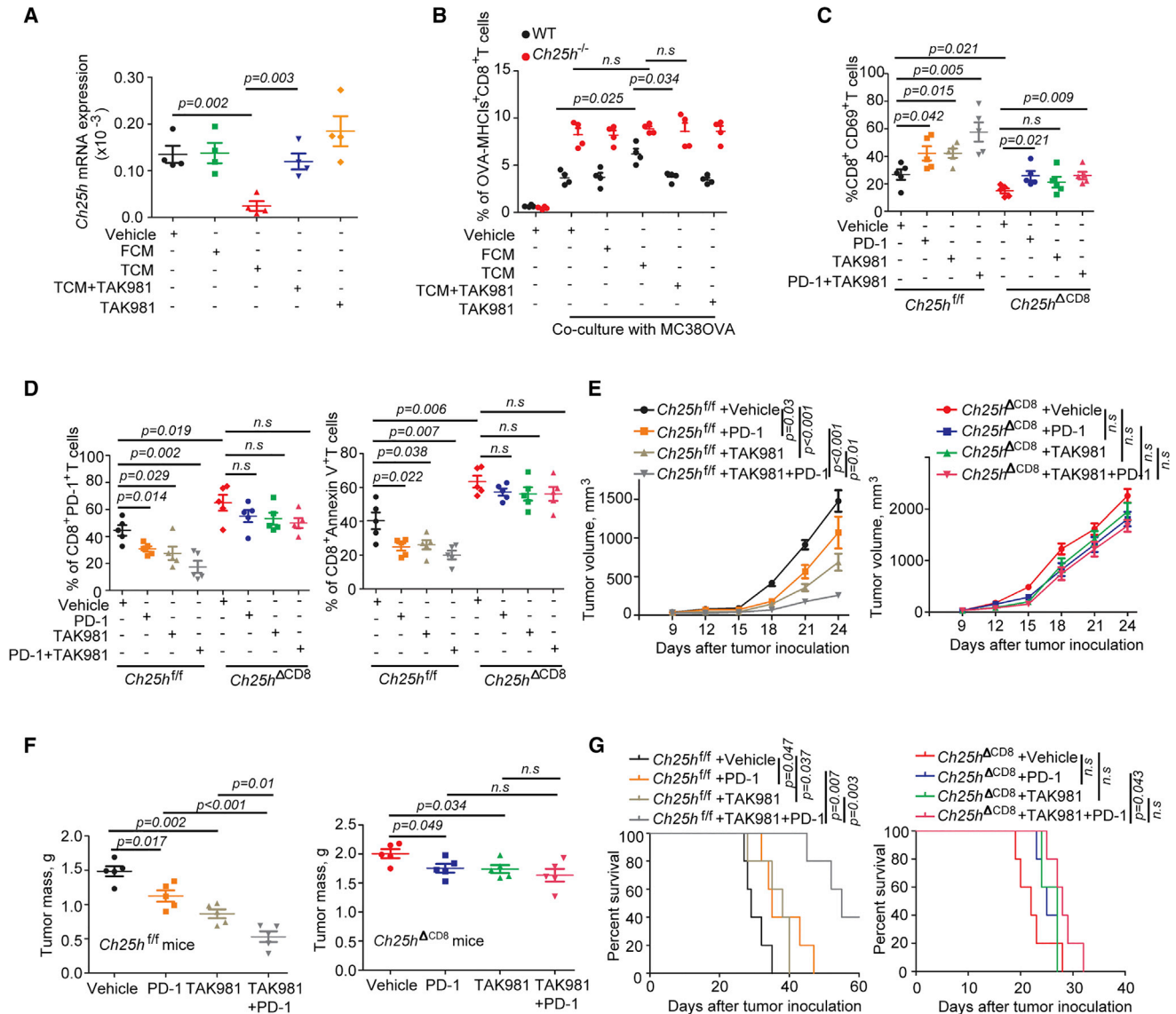


Figure 6. TAK981 sumoylation inhibitor upregulates CH25H, inhibits trogocytosis, and augments CAR T viability and anti-tumor activities

(A) qPCR analysis of *Ch25h* expression in CTLs treated with FCM or TCM in the presence or absence of TAK981 (0.1 μ M for 8 h) (n = 4).
 (B) Transfer of OVA-MHC-I complexes from MC38OVA cells onto WT or *Ch25h*^{-/-} OT-I CTLs pre-treated or not with FCM or TCM (in presence or absence of 0.1 μ M TAK981) (n = 4).
 (C) Expression of CD69 by the intratumoral CTLs isolated from MC38 tumors that grew in *Ch25h*^{fl/fl} or *Ch25h* ^{Δ CD8} mice treated with vehicle (PBS), anti-PD-1 antibody (i.p., 5 mg/kg every 4 days) and/or TAK981 (i.v., 15 mg/kg once a week) as indicated (n = 5).
 (D) Expression of PD-1 and annexin V by the intratumoral CTLs from experiments described in (C) (n = 5).
 (E) Volume of MC38 tumors from experiments described in (C) (n = 5).
 (F) Weight of MC38 tumors from experiments described in (C) (n = 5).
 (G) Survival analysis of animals from experiments described in (C). Mice were euthanized when tumor volume reached \sim 2,000 mm³ (n = 5).
 Data are presented as mean \pm SEM. Statistical analysis was performed using 1-way ANOVA with Tukey's multiple-comparison test (A, B, C, D, and F) or 2-way ANOVA with Sidak's multiple-comparison test (E) or Kaplan-Meier test (G). n.s., not significant.
 See also Figure S6.

ATF3-CH25H axis. Finally, 25HC also acts as a negative regulator of the cell membrane cholesterol (Kandutsch and Chen, 1975), and reduction of cholesterol levels in CD8⁺ T cells prevents their exhaustion in the tumor microenvironment (Ma et al., 2019).

It is plausible that suppressing CH25H expression and stimulating effector trogocytosis might represent an evolutionarily important mechanism that attenuates the function of immune system. Such mechanisms may plausibly play a protective role to minimize tissue damage during inflammation and T cell-driven

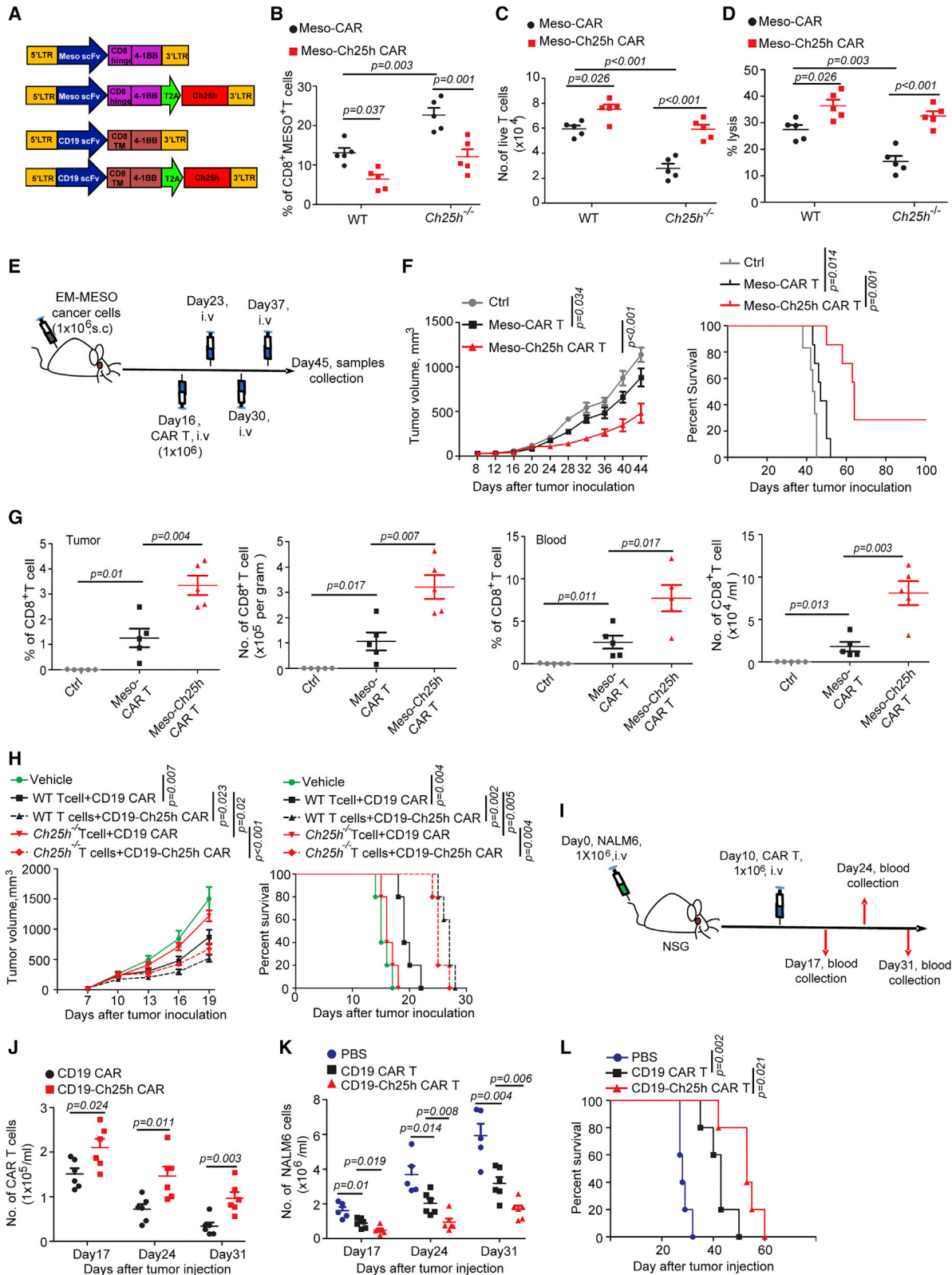


Figure 7. CARs designed to re-express CH25H inhibit trogocytosis and increase therapeutic efficacy

(A) Design of anti-Meso-CAR, anti-Meso-Ch25h CAR, anti-CD19 CAR, and anti-CD19-Ch25h CAR constructs.

(B) Transfer of MESO from EM-Meso-GFP-Luc cells onto WT or CH25H-null anti-MESO or anti-MESO-Ch25h CAR T cells co-cultured for 4 h (n = 5).

(legend continued on next page)

autoimmune reactions. If that is true, it would not be the first time, when such protective mechanism is appropriated by a growing tumor to evade the T cell immunity and perhaps even develop a resistance to therapies that involve adoptive transfer of CTLs.

The trogocytosis-driven loss of antigen on target malignant cells that persist following an encounter with CTL (Hamieh et al., 2019) is likely temporary and reversible. Nevertheless, these events provide cancer cells with a window of opportunity for evading future killing through numerous mechanisms including downregulation of MHC-I (Jhunjhunwala et al., 2021), immunoeediting and loss of antigen expression (Zheng et al., 2019), production of additional immune-suppressive ligands and substances (e.g., PD-L1, adenosine, or tumor-derived extracellular vesicles; Becker et al., 2013; Gajewski et al., 2006; Whiteside, 2016), and other mechanisms. Restricting trogocytosis by re-expression of CH25H in CTLs and production of 25HC is expected to close this temporal window and prevent resistance to adoptive cell transfer therapies.

Besides masking malignant cells through decreasing antigen density, trogocytosis also affects CTLs themselves. A number of consequences ensue for an effector CTL that did not manage to kill target malignant cell and, instead, engaged in trogocytosis. Among these consequences are exposure to other CTLs and subsequent fratricide as well as trogocytosis-associated exhaustion described for both CAR T and natural effector CD8⁺ T cells (Hamieh et al., 2019; Huang et al., 1999). It is likely that both consequences richly contribute to reduced killing capacity of CTLs *in vitro* and decreased efficacy of these cells in the therapeutic settings. Future studies are warranted to understand how trogocytosis affects the killing activities of a CTL coupled with a target malignant cell. Furthermore, at the present time, we cannot entirely rule out that changes in CTLs viability and activity are indirect and perhaps propensity for trogocytosis may reflect other ATF3/CH25H-dependent mechanisms that occur in parallel, but not conferred by trogocytosis.

Regardless of the mechanism, current data suggest that restricting trogocytosis via inducing CH25H expression using small molecule agents or CAR constructs engineered to re-express CH25H in CTLs should lessen the time and chance for malignant cells to undergo immunoeediting and generate the immune-suppressive tumor microenvironment. This strategy should increase the efficacy of anti-cancer therapies involving

adoptive transfer of CTLs such as CAR T cells (as demonstrated in Figure 7).

25HC robustly inhibits trogocytosis *in vitro*; however, this oxysterol has limited stability and suboptimal bioavailability (Li et al., 2017), complicating its use *in vivo*. Data presented here reveal that sumoylation inhibitor TAK981 can decrease the extent of trogocytosis (Figure 6). This agent acts to re-activate the anti-tumor immunity (Lightcap et al., 2021) and is currently investigated in several oncology clinical trials (including NCT03648372, NCT04074330, NCT04776018, and NCT04381650). Our current data suggest that the efficacy of TAK981 relates to its ability to prevent downregulation of CH25H expression in the CD8⁺ T cells (Figure 6). While clinical testing of this agent and its combinations with different types of immune therapies is underway, it is important to stratify these efforts and focus on scenarios where trogocytosis in CTLs acts to promote tumor growth. Otherwise, indiscriminate suppression of trogocytosis may negate the benefits of trogocytosis-mediated cross-priming (Hudrisier et al., 2005; Uzana et al., 2015; Zhang et al., 2008) and of trogocytosis-dependent anti-tumor effects elicited by neutrophils or macrophages (Horner et al., 2007; Stasilojc et al., 2016; Velmurugan et al., 2016). Besides these considerations, protein sumoylation affect numerous important cellular processes and continuous use of sumoylation inhibitors may complicate the efforts to manage oncological disease due to toxicity.

Given these considerations, it would be more attractive to restrict the inhibition of trogocytosis to CTLs. Engineering human CAR T cells that either lack ATF3 (for example, via CRISPR/Cas9-driven knockout) or re-express CH25H would represent such strategy. However, ATF3 is a key transcription factor that regulates many important genes and whose effects on tumor growth and progression are complex (Hai et al., 2010). Thus, we preferred to design a third-generation armored CAR that co-expresses CH25H to guard against its downregulation in the tumor microenvironment. Our study demonstrates a proof of principle that such approach works. Expression of CH25H within CAR indeed protects CAR T cells from trogocytosis and associated decrease in survival and activity and increases therapeutic efficacy of mouse and human CAR T cells (Figure 7). Future clinical studies will determine the utility of this CAR design in patients with solid tumors and leukemia.

(C) Numbers of live WT or CH25H-null anti-MESO or anti-MESO-Ch25h CAR T cells after co-culture with EM-Meso-GFP-Luc target cells for 8 h (n = 5).

(D) Luciferase-based analysis of killing of EM-Meso-GFP-Luc target cells by WT or CH25H-null anti-MESO or anti-MESO-Ch25h CAR T cells (n = 5).

(E) A schematic of experiment for comparing the efficacy of anti-Meso-CAR and anti-MESO-Ch25 h T cells *in vivo*.

(F) Volume of EM-Meso-GFP-Luc tumors (inoculated s.c. at 1×10^6) in NSG mice treated with vehicle, Meso-CAR T cells, or Meso-Ch25h CAR T cells as indicated in ϵ (n = 6). Kaplan-Meier survival analysis of survival of tumor-bearing mice (euthanized when tumors reached 1,000 mm³) is shown on the right (n = 7).

(G) Quantification of percentage (left) and absolute numbers (right) of CD3⁺CD8⁺ T cells (i.e., CAR T cells) in EM-Meso-GFP-Luc tumors (upper panels) and blood (bottom panels) from NSG mice treated as in (E) (n = 5).

(H) Volume of B16F10-hCD19 tumors (inoculated s.c. at 0.3×10^6) growing in *Rag1*^{-/-} mice treated with vehicle or indicated CAR T cells generated from WT or *Ch25h*^{-/-} splenocytes using anti-CD19 CAR or anti-CD19-Ch25h CAR constructs as indicated (upper panel). Kaplan-Meier survival analysis of survival of tumor-bearing mice (euthanized when tumors reached 1,000 mm³) is shown on the bottom (n = 5).

(I) A schematic of experiment for comparing the efficacy of human anti-CD19 and anti-CD19-Ch25h CAR T cells in the model of NALM6 acute lymphoblastic leukemia in NSG mice.

(J) Numbers of indicated CAR T cells in blood of NSG mice at day 17, 24, and 31 after injection of NALM6 leukemic cells (n = 6).

(K) Numbers of NALM6 cell in blood of NSG mice at day 17, 24, and 31 after injection of NALM6 leukemic cells (n = 5 or 6).

(L) Survival analysis of NALM6 leukemia cells-bearing mice treated with PBS or indicated CAR T cells (n = 5).

Data are presented as mean \pm SEM. Statistical analysis was performed using 1-way ANOVA with Tukey's multiple-comparison test (B, C, and D) or 2-way ANOVA with Sidak's multiple-comparison test (F, H, and L) or Kaplan-Meier test (F, H, and L) or 2-tailed Students' t test (G, J, and K). n.s., not significant. See also Figure S7.

Limitations of study

Data presented here demonstrate the importance of the ATF3-CH25H regulatory axis in stimulation of the effector trogocytosis in the tumor microenvironment. Consistent with previous reports regarding the consequences of effector trogocytosis in B cell leukemia (Hamieh et al., 2019), our results obtained in several solid tumor models reveal that trogocytosis is associated with decreased viability and impaired activity of CTLs. Accordingly, our results demonstrate the importance of activation of the ATF3-CH25H pathway in restricting the capacity of anti-tumor effects elicited by endogenous and CAR-bearing CTLs. These data support a model where induction of ATF3 and suppression of CH25H in the intratumoral CTLs stimulate trogocytosis and undermine activities and viability of these CTLs. However, additional ATF3-CH25H-dependent and independent mechanisms related to the antigen exposure are likely to contribute to inactivation and demise of the trogocytosis-experienced CTLs in addition to trogocytosis itself. In addition, further studies are required to elucidate putative LXR-dependent and LXR-independent mechanisms by which 25HC restricts the ability of CTLs to undergo trogocytosis. Furthermore, given that isolation of apoptosis-prone trogocytosis-experienced CTLs from human tumors is increasingly challenging, a proper assessment of the extent of effector trogocytosis in human cancers and association of these events with infiltration of CD8⁺ cytotoxic lymphocytes and with tumor growth and progression requires future technological advances and additional studies.

STAR★METHODS

Detailed methods are provided in the online version of this paper and include the following:

- **KEY RESOURCES TABLE**
- **RESOURCE AVAILABILITY**
 - Lead contact
 - Materials availability statement
 - Data and code availability
- **EXPERIMENTAL MODEL AND SUBJECT DETAILS**
 - Study approvals
 - Animal studies
 - Cell culture and conditioned media
- **METHOD DETAILS**
 - CAR T cells: Vector generation, T cell isolation, expansion, and CAR T cells generation
 - Cytotoxicity, viability and exhaustion assays
 - Flow cytometry of tumors or spleens, immunofluorescence, immunoprecipitation and immunoblotting
 - Flow cytometry analysis of trogocytosis
 - Quantitative real-time PCR
 - Chromatin immunoprecipitation (ChIP) analysis
 - Tumorigenesis studies
 - Combination therapy and CAR T therapies
- **TROGOCYTOSIS AND VIABILITY ASSAY IN VIVO**
 - RNA sequencing analysis
 - Metabolomics studies
- **QUANTIFICATION AND STATISTICAL ANALYSIS**
 - Human databases analysis

SUPPLEMENTAL INFORMATION

Supplemental information can be found online at <https://doi.org/10.1016/j.cmet.2022.08.007>.

ACKNOWLEDGMENTS

This work was supported by the by the NIH/NCI R01 grants nos. CA247803 and R01 CA240814 (to S.Y.F.) and P01 grant P01 CA165997 (to J.A.D., C.K., A.W., and S.Y.F.). We are grateful for an additional support from T32 CA115299 (to N.M.). We thank the Human Immunology Core at the University of Pennsylvania for providing purified human leukocyte subsets for our research. We thank Clara Malekshahi for technical assistance; Dr. Bang Wang (Karolinska Institute) for help with analysis of RNA sequencing data; Dr. Evgeniy B. Eruslanov (University of Pennsylvania) for valuable advice; and Drs. Michael Milone, Malay Halder, Ben Stanger, Andy Minn, and Edmund K. Moon (University of Pennsylvania); Tsonwin Hai (Ohio State University); and Susan Ostrand-Rosenberg (University of Maryland) for the reagents. We are also grateful to Drs. Andrei Thomas-Tikhonenko (University of Pennsylvania) and Tsonwin Hai (Ohio State University) for critical reading of the manuscript and to Dr. A. Gamero (Temple University) and the members of the Koumenis, Minn, Chow, and Fuchs laboratories (University of Pennsylvania) for suggestions and advice.

AUTHOR CONTRIBUTIONS

S.Y.F., Z.L., N.M., A.W., C.K., and J.A.D. conceived the study and designed the research. Z.L. and N.M. performed most of the experiments with the help of J.C., V.S.T., H.Z., G.D.R., and A.T. D.P.B., Z.M., and S.S.G. performed bioinformatics analyses. A.B. and S.G. provided critically important reagents and helped with experimental design, analysis, data interpretation, and writing. S.Y.F. and Z.L. wrote the manuscript with the help from all authors.

DECLARATION OF INTERESTS

A.B. and G.S. were employees of and stockholders in Millennium Pharmaceuticals, Inc., a wholly owned subsidiary of Takeda Pharmaceutical Company Limited producing TAK981, while engaged in the research project. Z.L., N.M., and S.Y.F. are listed as inventors on The University of Pennsylvania's patent application related to the matter described in this manuscript.

Received: December 28, 2021

Revised: May 31, 2022

Accepted: August 11, 2022

Published: September 6, 2022

REFERENCES

- Ahmed, K.A., Munegowda, M.A., Xie, Y., and Xiang, J. (2008). Intercellular trogocytosis plays an important role in modulation of immune responses. *Cell. Mol. Immunol.* *5*, 261–269. <https://doi.org/10.1038/cmi.2008.32>.
- Amorim, C.F., Novais, F.O., Nguyen, B.T., Mistic, A.M., Carvalho, L.P., Carvalho, E.M., Beiting, D.P., and Scott, P. (2019). Variable gene expression and parasite load predict treatment outcome in cutaneous leishmaniasis. *Sci. Transl. Med.* *11*, eaax4204. <https://doi.org/10.1126/scitranslmed.aax4204>.
- Anggakusuma, Romero-Brey, I., Berger, C., Colpitts, C.C., Boldanova, T., Engelmann, M., Todt, D., Perin, P.M., Behrendt, P., Vondran, F.W.R., et al. (2015). Interferon-inducible cholesterol-25-hydroxylase restricts hepatitis C virus replication through blockage of membranous web formation. *Hepatology* *62*, 702–714. <https://doi.org/10.1002/hep.27913>.
- Baek, A.E., Yu, Y.R.A., He, S., Wardell, S.E., Chang, C.Y., Kwon, S., Pillai, R.V., McDowell, H.B., Thompson, J.W., Dubois, L.G., et al. (2017). The cholesterol metabolite 27 hydroxycholesterol facilitates breast cancer metastasis through its actions on immune cells. *Nat. Commun.* *8*, 864. <https://doi.org/10.1038/s41467-017-00910-z>.
- Barysch, S.V., Stankovic-Valentin, N., Miedema, T., Karaca, S., Doppel, J., Nait Achour, T., Vasudeva, A., Wolf, L., Sticht, C., Urlaub, H., and Melchior,

- F. (2021). Transient deSUMOylation of IRF2BP proteins controls early transcription in EGFR signaling. *EMBO Rep.* 22, e49651. <https://doi.org/10.15252/embr.201949651>.
- Becker, J.C., Andersen, M.H., Schrama, D., and Thor Straten, P. (2013). Immune-suppressive properties of the tumor microenvironment. *Cancer Immunol. Immunother.* 62, 1137–1148. <https://doi.org/10.1007/s00262-013-1434-6>.
- Choudhuri, K., Llodrá, J., Roth, E.W., Tsai, J., Gordo, S., Wucherpfennig, K.W., Kam, L.C., Stokes, D.L., and Dustin, M.L. (2014). Polarized release of T-cell-receptor-enriched microvesicles at the immunological synapse. *Nature* 507, 118–123. <https://doi.org/10.1038/nature12951>.
- Cyster, J.G., Dang, E.V., Reboldi, A., and Yi, T. (2014). 25-Hydroxycholesterols in innate and adaptive immunity. *Nat. Rev. Immunol.* 14, 731–743. <https://doi.org/10.1038/nri3755>.
- Dance, A. (2019). Core Concept: Cells nibble one another via the under-appreciated process of trogocytosis. *Proc. Natl. Acad. Sci. USA* 116, 17608–17610. <https://doi.org/10.1073/pnas.1912252116>.
- DeBarber, A.E., Lütjohann, D., Merckens, L., and Steiner, R.D. (2008). Liquid chromatography-tandem mass spectrometry determination of plasma 24S-hydroxycholesterol with chromatographic separation of 25-hydroxycholesterol. *Anal. Biochem.* 387, 151–153. <https://doi.org/10.1016/j.ab.2008.05.037>.
- Decque, A., Joffre, O., Magalhaes, J.G., Cossec, J.C., Blecher-Gonen, R., Lapaquette, P., Silvín, A., Manel, N., Joubert, P.E., Seeler, J.S., et al. (2016). Sumoylation coordinates the repression of inflammatory and anti-viral gene-expression programs during innate sensing. *Nat. Immunol.* 17, 140–149. <https://doi.org/10.1038/ni.3342>.
- Gajewski, T.F., Meng, Y., Blank, C., Brown, I., Kacha, A., Kline, J., and Harlin, H. (2006). Immune resistance orchestrated by the tumor microenvironment. *Immunol. Rev.* 213, 131–145. <https://doi.org/10.1111/j.1600-065X.2006.00442.x>.
- Geiss-Friedlander, R., and Melchior, F. (2007). Concepts in sumoylation: a decade on. *Nat. Rev. Mol. Cell Biol.* 8, 947–956. <https://doi.org/10.1038/nrm2293>.
- Gold, E.S., Ramsey, S.A., Sartain, M.J., Selinummi, J., Podolsky, I., Rodriguez, D.J., Moritz, R.L., and Aderem, A. (2012). ATF3 protects against atherosclerosis by suppressing 25-hydroxycholesterol-induced lipid body formation. *J. Exp. Med.* 209, 807–817. <https://doi.org/10.1084/jem.20111202>.
- Gui, J., Zahedi, F., Ortiz, A., Cho, C., Katlinski, K.V., Alicea-Torres, K., Li, J., Todd, L., Zhang, H., Beiting, D.P., et al. (2020). Activation of p38alpha stress-activated protein kinase drives the formation of the pre-metastatic niche in the lungs. *Nat. Cancer* 1, 603–619. <https://doi.org/10.1038/s43018-020-0064-0>.
- Hai, T., Wolford, C.C., and Chang, Y.S. (2010). ATF3, a hub of the cellular adaptive-response network, in the pathogenesis of diseases: is modulation of inflammation a unifying component? *Gene Expr.* 15, 1–11. <https://doi.org/10.3727/105221610x12819686555015>.
- Hamieh, M., Dobrin, A., Cabriolu, A., van der Stegen, S.J.C., Giavridis, T., Mansilla-Soto, J., Eyquem, J., Zhao, Z., Whitlock, B.M., Miele, M.M., et al. (2019). CAR T cell trogocytosis and cooperative killing regulate tumour antigen escape. *Nature* 568, 112–116. <https://doi.org/10.1038/s41586-019-1054-1>.
- Horner, H., Frank, C., Dechant, C., Repp, R., Glennie, M., Herrmann, M., and Stockmeyer, B. (2007). Intimate cell conjugate formation and exchange of membrane lipids precede apoptosis induction in target cells during antibody-dependent, granulocyte-mediated cytotoxicity. *J. Immunol.* 179, 337–345. <https://doi.org/10.4049/jimmunol.179.1.337>.
- Huang, J.F., Yang, Y., Sepulveda, H., Shi, W., Hwang, I., Peterson, P.A., Jackson, M.R., Sprent, J., and Cai, Z. (1999). TCR-Mediated internalization of peptide-MHC complexes acquired by T cells. *Science* 286, 952–954. <https://doi.org/10.1126/science.286.5441.952>.
- Huangfu, W.C., Qian, J., Liu, C., Liu, J., Lokshin, A.E., Baker, D.P., Rui, H., and Fuchs, S.Y. (2012). Inflammatory signaling compromises cell responses to interferon alpha. *Oncogene* 31, 161–172. <https://doi.org/10.1038/onc.2011.221>.
- Hudrisier, D., Riond, J., Garidou, L., Duthoit, C., and Joly, E. (2005). T cell activation correlates with an increased proportion of antigen among the materials acquired from target cells. *Eur. J. Immunol.* 35, 2284–2294. <https://doi.org/10.1002/eji.200526266>.
- Jhunjhunwala, S., Hammer, C., and Delamarre, L. (2021). Antigen presentation in cancer: insights into tumour immunogenicity and immune evasion. *Nat. Rev. Cancer* 21, 298–312. <https://doi.org/10.1038/s41568-021-00339-z>.
- Kandutsch, A.A., and Chen, H.W. (1975). Regulation of sterol synthesis in cultured cells by oxygenated derivatives of cholesterol. *J. Cell. Physiol.* 85, 415–424. <https://doi.org/10.1002/jcp.1040850408>.
- Katlinskaya, Y.V., Katlinski, K.V., Lasri, A., Li, N., Beiting, D.P., Durham, A.C., Yang, T., Pikarsky, E., Lengner, C.J., Johnson, F.B., et al. (2016). Type I Interferons Control Proliferation and Function of the Intestinal Epithelium. *Mol. Cell Biol.* 36, 1124–1135. <https://doi.org/10.1128/MCB.00988-15>.
- Katlinski, K.V., Gui, J., Katlinskaya, Y.V., Ortiz, A., Chakraborty, R., Bhattacharya, S., Carbone, C.J., Beiting, D.P., Gironde, M.A., Peck, A.R., et al. (2017). Inactivation of Interferon Receptor Promotes the Establishment of Immune Privileged Tumor Microenvironment. *Cancer Cell* 31, 194–207. <https://doi.org/10.1016/j.ccell.2017.01.004>.
- Labzin, L.I., Schmidt, S.V., Masters, S.L., Beyer, M., Krebs, W., Klee, K., Stahl, R., Lütjohann, D., Schultze, J.L., Latz, E., and De Nardo, D. (2015). ATF3 Is a Key Regulator of Macrophage IFN Responses. *J. Immunol.* 195, 4446–4455. <https://doi.org/10.4049/jimmunol.1500204>.
- Li, C., Deng, Y.Q., Wang, S., Ma, F., Aliyari, R., Huang, X.Y., Zhang, N.N., Watanabe, M., Dong, H.L., Liu, P., et al. (2017). 25-Hydroxycholesterol Protects Host against Zika Virus Infection and Its Associated Microcephaly in a Mouse Model. *Immunity* 46, 446–456. <https://doi.org/10.1016/j.immuni.2017.02.012>.
- Li, T., Fu, J., Zeng, Z., Cohen, D., Li, J., Chen, Q., Li, B., and Liu, X.S. (2020). TIMER2.0 for analysis of tumor-infiltrating immune cells. *Nucleic Acids Res.* 48, W509–W514. <https://doi.org/10.1093/nar/gkaa407>.
- Lightcap, E.S., Yu, P., Grossman, S., Song, K., Khattar, M., Xega, K., He, X., Gavin, J.M., Imaichi, H., Garnsey, J.J., et al. (2021). A small-molecule SUMOylation inhibitor activates antitumor immune responses and potentiates immune therapies in preclinical models. *Sci. Transl. Med.* 13, eaba7791. <https://doi.org/10.1126/scitranslmed.aba7791>.
- Liu, X., Bao, X., Hu, M., Chang, H., Jiao, M., Cheng, J., Xie, L., Huang, Q., Li, F., and Li, C.Y. (2020). Inhibition of PCSK9 potentiates immune checkpoint therapy for cancer. *Nature* 588, 693–698. <https://doi.org/10.1038/s41586-020-2911-7>.
- Lu, Z., Ortiz, A., Verginadis, I.I., Peck, A.R., Zahedi, F., Cho, C., Yu, P., DeRita, R.M., Zhang, H., Kubanoff, R., et al. (2021). Regulation of intercellular biomolecule transfer-driven tumor angiogenesis and responses to anticancer therapies. *J. Clin. Invest.* 131, 144225. <https://doi.org/10.1172/JCI144225>.
- Lyst, M.J., and Stancheva, I. (2007). A role for SUMO modification in transcriptional repression and activation. *Biochem. Soc. Trans.* 35, 1389–1392. <https://doi.org/10.1042/BST0351389>.
- Ma, X., Bi, E., Lu, Y., Su, P., Huang, C., Liu, L., Wang, Q., Yang, M., Kalady, M.F., Qian, J., et al. (2019). Cholesterol Induces CD8(+) T Cell Exhaustion in the Tumor Microenvironment. *Cell Metab.* 30, 143–156.e5. <https://doi.org/10.1016/j.cmet.2019.04.002>.
- Milone, M.C., Fish, J.D., Carpenito, C., Carroll, R.G., Binder, G.K., Teachey, D., Samanta, M., Lakhali, M., Gloss, B., Danet-Desnoyers, G., et al. (2009). Chimeric receptors containing CD137 signal transduction domains mediate enhanced survival of T cells and increased antileukemic efficacy in vivo. *Mol. Ther.* 17, 1453–1464. <https://doi.org/10.1038/mt.2009.83>.
- Miyake, K., and Karasuyama, H. (2021). The role of trogocytosis in the modulation of immune cell functions. *Cells* 10. <https://doi.org/10.3390/cells10051255>.
- Nakayama, M., Hori, A., Toyoura, S., and Yamaguchi, S.I. (2021). Shaping of T Cell Functions by Trogocytosis. *Cells* 10. <https://doi.org/10.3390/cells10051155>.
- Ortiz, A., Gui, J., Zahedi, F., Yu, P., Cho, C., Bhattacharya, S., Carbone, C.J., Yu, Q., Katlinski, K.V., Katlinskaya, Y.V., et al. (2019). An interferon-driven oxysterol-based defense against tumor-derived extracellular vesicles. *Cancer Cell* 35, 33–45.e6. <https://doi.org/10.1016/j.ccell.2018.12.001>.

- Park, S.J., Yoon, B.H., Kim, S.K., and Kim, S.Y. (2019). GENT2: an updated gene expression database for normal and tumor tissues. *BMC Med. Genomics* 12, 101. <https://doi.org/10.1186/s12920-019-0514-7>.
- Rabinovich, G.A., Gabrilovich, D., and Sotomayor, E.M. (2007). Immunosuppressive strategies that are mediated by tumor cells. *Annu. Rev. Immunol.* 25, 267–296. <https://doi.org/10.1146/annurev.immunol.25.022106.141609>.
- Rechavi, O., Goldstein, I., and Kloog, Y. (2009). Intercellular exchange of proteins: the immune cell habit of sharing. *FEBS Lett.* 583, 1792–1799. <https://doi.org/10.1016/j.febslet.2009.03.014>.
- Stasić, G., Österborg, A., Blom, A.M., and Okrój, M. (2016). New perspectives on complement mediated immunotherapy. *Cancer Treat Rev.* 45, 68–75. <https://doi.org/10.1016/j.ctrv.2016.02.009>.
- Takáts, Z., Wiseman, J.M., Gologan, B., and Cooks, R.G. (2004). Mass spectrometry sampling under ambient conditions with desorption electrospray ionization. *Science* 306, 471–473. <https://doi.org/10.1126/science.1104404>.
- Tambellini, N.P., Zarembek, V., Turner, R.J., and Weljie, A.M. (2013). Evaluation of extraction protocols for simultaneous polar and non-polar yeast metabolite analysis using multivariate projection methods. *Metabolites* 3, 592–605. <https://doi.org/10.3390/metabo3030592>.
- Uzana, R., Eisenberg, G., Merims, S., Frankenburg, S., Pato, A., Yefenof, E., Engelstein, R., Peretz, T., Machlenkin, A., and Lotem, M. (2015). Human T cell crosstalk is induced by tumor membrane transfer. *PLoS One* 10, e0118244. <https://doi.org/10.1371/journal.pone.0118244>.
- Velmurugan, R., Challa, D.K., Ram, S., Ober, R.J., and Ward, E.S. (2016). Macrophage-Mediated Trophocytosis Leads to Death of Antibody-Opsonized Tumor Cells. *Mol. Cancer Ther.* 15, 1879–1889. <https://doi.org/10.1158/1535-7163.MCT-15-0335>.
- Wang, C.M., Brennan, V.C., Gutierrez, N.M., Wang, X., Wang, L., and Yang, W.H. (2013). SUMOylation of ATF3 alters its transcriptional activity on regulation of TP53 gene. *J. Cell. Biochem.* 114, 589–598. <https://doi.org/10.1002/jcb.24396>.
- Whiteside, T.L. (2016). Exosomes and tumor-mediated immune suppression. *J. Clin. Invest.* 126, 1216–1223. <https://doi.org/10.1172/JCI81136>.
- Wolford, C.C., McConoughey, S.J., Jalgaonkar, S.P., Leon, M., Merchant, A.S., Dominick, J.L., Yin, X., Chang, Y., Zmuda, E.J., O'Toole, S.A., et al. (2013). Transcription factor ATF3 links host adaptive response to breast cancer metastasis. *J. Clin. Invest.* 123, 2893–2906. <https://doi.org/10.1172/JCI64410>.
- Yang, S.T., Kreutzberger, A.J.B., Lee, J., Kiessling, V., and Tamm, L.K. (2016). The role of cholesterol in membrane fusion. *Chem. Phys. Lipids* 199, 136–143. <https://doi.org/10.1016/j.chemphyslip.2016.05.003>.
- Zang, R., Case, J.B., Yutuc, E., Ma, X., Shen, S., Gomez Castro, M.F., Liu, Z., Zeng, Q., Zhao, H., Son, J., et al. (2020). Cholesterol 25-hydroxylase suppresses SARS-CoV-2 replication by blocking membrane fusion. *Proc. Natl. Acad. Sci. USA* 117, 32105–32113. <https://doi.org/10.1073/pnas.2012197117>.
- Zhang, H., Yu, P., Tomar, V.S., Chen, X., Atherton, M.J., Lu, Z., Zhang, H.G., Li, S., Ortiz, A., Gui, J., et al. (2022). Targeting PARP11 to avert immunosuppression and improve CAR T therapy in solid tumors. *Nat. Cancer* 3, 808–820. <https://doi.org/10.1038/s43018-022-00383-0>.
- Zhang, Q.J., Li, X.L., Wang, D., Huang, X.C., Mathis, J.M., Duan, W.M., Knight, D., Shi, R., Glass, J., Zhang, D.Q., et al. (2008). Trophocytosis of MHC-I/peptide complexes derived from tumors and infected cells enhances dendritic cell cross-priming and promotes adaptive T cell responses. *PLoS One* 3, e3097. <https://doi.org/10.1371/journal.pone.0003097>.
- Zheng, S., Asnani, M., and Thomas-Tikhonenko, A. (2019). Escape From ALL-CARTaz: leukemia immunoediting in the age of chimeric antigen receptors. *Cancer J.* 25, 217–222. <https://doi.org/10.1097/PPO.0000000000000381>.

STAR★METHODS

KEY RESOURCES TABLE

REAGENT or RESOURCE	SOURCE	IDENTIFIER
<i>Antibodies</i>		
anti- mouse CD8-APC/Cy7	Biolegend	Cat# 100714; RRID: AB_312753
anti-mouse CD69-PE	Biolegend	Cat# 104507; RRID: AB_313110
anti-mouse PD-1-BV605	BioLegend	Cat# 135219; RRID: AB_11125371
anti-mouse LAG3-PE/Cy7	BioLegend	Cat# 125226; RRID: AB_2715764
anti-mouse CD366-BV421	BioLegend	Cat# 134019; RRID: AB_2814028
anti-mouse Annexin V-FITC	BioLegend	Cat# 640906; RRID: AB_2561292
anti-mouse CD45-APC/Cy7	BioLegend	Cat# 157203; RRID: AB_2876533
anti-mouse CD3-PE	BioLegend	Cat# 100206; RRID: AB_312663
anti-mouse CD8-AF700	BioLegend	Cat# 100730; RRID: AB_493703
anti-mouse CD69-BV421	BioLegend	Cat# 104545; RRID: AB_2686969
anti-mouse PD-1-PE/Cy7	BioLegend	Cat# 109110; RRID: AB_572017
anti-mouse LAG3-BV650	BioLegend	Cat# 125227; RRID: AB_2687209
Anti-mouse Annexin V-APC	BioLegend	Cat# 640941; RRID: AB_2616657
anti-hCD19-APC	Biolegend	Cat# 392504; RRID: AB_2728416
anti-human CD19 CAR-PE	Acrobiosystems	Cat#FM3-HPY53
anti-human CD8-PE/Cy7	BioLegend	Cat# 344750; RRID: AB_2687201
anti-mouse CD4-APC/Cy7	BioLegend	Cat# 100414; RRID: AB_312699
anti-mouse CD19-PE	BioLegend	Cat# 115507; RRID: AB_313642
anti-mouse NK1.1-APC	BioLegend	Cat# 108709; RRID: AB_313396
Biotin anti-mouse CD3	BioLegend	Cat# 100243; RRID: AB_2563946
Alexa Fluor-594 streptavidin	BioLegend	N/A
Alexa Fluor-488 anti-mouse CD8	BioLegend	Cat# 100723; RRID: AB_389304
Rabbit anti-mouse ATF3 antibody	Cell Signaling	Cat#18665S
Anti-mouse SUMO1	Invitrogen	Cat# 33-2400; RRID: AB_2533109
VeriBlot for IP Detection Reagent HRP	Abcam	N/A
Goat anti-mouse HRP-conjugated antibody	Cell Signaling	Cat# 7076S
Rat anti-mouse β -tubulin antibody	Cell Signaling	Cat# 2146

(Continued on next page)

Continued

REAGENT or RESOURCE	SOURCE	IDENTIFIER
PE-anti-mouse H-2K ^b binds to SIINFEKL antibody	BioLegend	Cat# 141603; RRID: AB_10897938
Recombinant Anti-Mesothelin antibody	Abcam	Cat# ab196235
Biological samples		
Healthy human peripheral T cells	Human Immunology Core at the University of Pennsylvania	N/A
Chemicals, peptides, and recombinant proteins		
Prostaglandin E2	Sigma	Cat# P0409
DMSO	Sigma	Cat# 20-139
VEGF165	Sigma	Cat# V5765
1,1'-dioctadecyl-3,3',3'-tetramethylindodicarbocyanine	Biotium	Cat# 60014
Latrunculin A	Sigma	Cat# L5163
25-hydroxycholesterol	Sigma	Cat# H1015
GW3965	Sigma	Cat# G6295
Golgi stop	BD	Cat# BDB554724
Transwell Chambers	Millipore	Cat# CLS3422-48EA
DNase I	Roche	Cat# 10104159001
Collagenase D	Roche	Cat# 11088882001
Percoll	Sigma	Cat# 17-0891-01
Lymphoprep™	Stem Cell	Cat# 07851
Recombinant human IL-2	Sigma	Cat# I0523
Ovalbumin (257-264) chicken	Sigma	Cat# S7951
Anti-PD-1	Bio X cell	Cat# BE0146 Clone: RMP1-14
CFSE	Biolegend	Cat# 79898
Dynabeads™ Mouse T-Activator CD3/CD28	Gibco	Cat# 11453D
Dynabeads™ Human T-Activator CD3/CD28	Gibco	Cat# 11132D
CountBright™ Absolute Counting Beads	Invitrogen	Cat# C36950
Fetal Bovine Serum	Hyclone	Cat# SH30071.03
High-Capacity RNA-to-cDNA™ Kit	Applied Biosystems	Cat# 4387406
Gibco™ L-Glutamine	Gibco	Cat# 25-030-081
Intracellular Fix & Perm Buffer set	eBioscience	Cat# 88-8824
Lipofectamin2000	Invitrogen	Cat# 52887
Retronectin	Takara	Cat# T100B
RBC lysis buffer	Biolegend	Cat# 420302
Critical commercial assays		
ONE-Glo™ Luciferase Assay System	Promega	Cat# E6120
Power SYBR Green PCR Master Mix	Thermo Fisher	Cat# 4367659
SimpleChIP Plus Enzymatic Chromatin IP Kit	Cell Signaling	Cat# 9005S
RNeasy Kits	Qiagen	Cat# 74004
EasySep™ Mouse CD8 ⁺ T Cell Isolation Kit	Stem Cell	Cat# 19853
EasySep™ Mouse T Cell Isolation Kit	Stem Cell	Cat# 19851
EasySep™ Mouse CD4 ⁺ T Cell Isolation Kit	Stem Cell	Cat# 19852
Deposited data		
Bulk RNA-sequence data	This paper	GEO: GSE190702
Raw data	This paper	Data S1

(Continued on next page)

REAGENT or RESOURCE	SOURCE	IDENTIFIER
Continued		
Experimental models: Cell lines		
Human: Phoenix-ECO	ATCC	Cat# CRL-3214™
Mouse: MC38	ATCC	N/A
Mouse: MC38 OVA	Cancer Cell, 2017, 31: 194-207	N/A
Mouse: MC38-OVA-Luciferase	Nat Cancer 2022 May 30. https://doi.org/10.1038/s43018-022-00383-0	N/A
Mouse: Hepa1-6	ATCC	Cat# CRL-1830™
Mouse: B16F10	ATCC	Cat# CRL-6475™
Mouse: MH6499c4	Immunity 49, 178–193	N/A
Human: NALM6	ATCC	Cat# CRL-3273™
Human: EM-Meso-GFP-Luciferase	Oncoimmunology, 2018, VOL. 7, NO. 3, e1395997	N/A
Mouse: NIH 3T3	ATCC	Cat# CRL-1658™
Experimental models: Organisms/strains		
Mouse: WT C57BL/6	Jackson Laboratory	Cat# 000664
Mouse: <i>Ch25h</i> ^{-/-} C57BL/6	Jackson Laboratory	Cat# 016263
Mouse: <i>Ch25h</i> ^{ΔCDB} C57BL/6	This paper	N/A
Mouse: <i>Atf3</i> ^{ΔCDB} C57BL/6	This paper	N/A
Mouse: OT1 C57BL/6	Jackson Laboratory	Cat# 003831
Mouse: Rag1 ^{-/-} C57BL/6J	Jackson Laboratory	Cat# 002216
Mouse: NSG NOD/ShiLtJ	Jackson Laboratory	Cat# 005557
Oligonucleotides		
Primers for q-PCR, see Table S1	This paper	N/A
Recombinant DNA (plasmid)		
Lenti-p-EF1α-Meso-scFV	10.1073/pnas.0813101106.	N/A
Lenti-p-EF1α-Meso-scFV-T2A-Ch25h	This paper	N/A
Retro-p-CD19-scFV-BBZ-MSGV	10.1016/j.cell.2021.08.004.	N/A
Retro-p-CD19-scFV-BBZ-T2A-Ch25h MSGV	This paper	N/A
Software and algorithms		
Prism 9	GraphPad Prism9	https://www.graphpad.com/
FlowJo 7.6 version	FlowJo	https://www.flowjo.com/
Image J	Image J	https://imagej.nih.gov/ij/

RESOURCE AVAILABILITY

Lead contact

Further information and requests for resources and reagents should be directed to and will be fulfilled by the lead contact, Dr. Serge Y. Fuchs (syfuchs@upenn.edu).

Materials availability statement

Mouse lines and constructs generated in this study can be requested from the lead contact and obtained under appropriate MTA or/and license from the University of Pennsylvania.

Data and code availability

- Bulk RNA-seq data have been deposited at GEO (accession number: GSE190702) and are publicly available as of the date of publication. Accession numbers are also listed in the [key resources table](#). Original western blot images and all raw data used to create the graphs can be found in [Data S1](#) (contains uncropped scans of Western blots and original data related to [Figures 1, 2, 3, 4, 5, 6, and 7](#) and [S1–S4, S6 and S7](#))
- No original code was generated for all data in this study.
- Any additional information required to analyze the data reported in this study is available from the lead contact upon request.

EXPERIMENTAL MODEL AND SUBJECT DETAILS

Study approvals

Human T cells were previously collected from healthy female and male donors (of age of 18–55 years) by the Human Immunology Core at the University of Pennsylvania under informed consent and could not be directly or indirectly linked to individual human subjects. Use of these cells was approved for by IRB of the University of Pennsylvania. All animal experiments were approved by the Institutional Animal Care and Use Committee of the University of Pennsylvania and were carried out in accordance with the IACUC guidelines. All animals were kept in SPF (specific pathogen-free) facility accordance with American Association for Laboratory Animal Science guidelines. All mice had water *ad libitum* and were fed with regular food. Littermates from different cages were randomly assigned into different group and were exposed to the same environment.

Animal studies

NSG, WT, *Ch25h*^{-/-}, *Rag1*^{-/-}, Cd8 Cre and OT-I mice were purchased from Jackson Laboratory and used for study directly after importing into facility. The conditional *Ch25h* allele was created by flanking the single exon of the *Ch25h* gene with the loxP sites inserted into the non-conservative regions (Lu et al., 2021). OT-I WT and OT-I *Ch25h*^{-/-} mice were generated by crossing OT-I mice with WT or *Ch25h*^{-/-} mice. *Atf3*^{fl/fl} mice were previously described (Wolford et al., 2013) and kindly provided by Dr. Tsonwin Hai (Ohio State University). *Ch25h*^{ΔCD8} or *Atf3*^{ΔCD8} or *Ch25h;Atf3*^{ΔCD8} mice were generated by intercrossing *Cd8-Cre* mice with conditional *Ch25h*^{fl/fl} or *Atf3*^{fl/fl} mice.

All animal experiments were performed using both male and female littermates (mated in-house) of 6–8 weeks of age. All mice except NSG were in the C57BL/6J background. Mice were housed in a specific pathogen free (SPF) condition (12 h light/12 h dark cycle, temperature 20–25°C) and had free access to water and chow (ANIMAL SPECIALTIES AND PROVISIONS, Lab diet 5010). Animal health status was routinely checked by qualified veterinarians.

Cell culture and conditioned media

Human 293T cell and B16F10 cell were purchased from ATCC. NALM6 acute lymphoblastic leukemia (from Michael C. Milone, University of Pennsylvania), MC38 colon adenocarcinoma (from Susan Ostrand-Rosenberg, University of Maryland), B16F10-hCD19 melanoma (B16F10 melanoma stably expressing human CD19 - from Andy Minn, University of Pennsylvania), human EM-Meso-GFP-Luc cell line (from Edmund Moon, University of Pennsylvania), MH6499c4 pancreatic ductal adenocarcinoma (from Ben Stanger, University of Pennsylvania) and Hepa1-6 hepatocellular carcinoma (from Malay Haldar, University of Pennsylvania) were kindly gifted. MC38-OVA and MC-38OVA-luc cells were previously described (Katlinski et al., 2017; Zhang et al., 2022). B16F10-hCD19-luc melanoma cells were generated by stable expression of luciferase in B16F10-hCD19 cells. 293T cell and all cancer cells were cultured at 37°C with 5% CO₂ in DMEM including 10% heat-inactivated Fetal Bovine Serum (FBS), 100 U/ml penicillin-streptomycin and L-glutamine. Phoenix packaging cells (from ATCC) were maintained at 37°C with 5% CO₂ in RPMI-1640 including 10% heat-inactivated Fetal Bovine Serum (FBS), 50 U/ml penicillin-streptomycin and L-glutamine. Tumor-condition medium (TCM) and NIH3T3 fibroblast-conditioned media (FCM) was prepared as previously reported (Gui et al., 2020). Mouse intestinal epithelial cells were obtained and cultured as previously described (Katlinskaya et al., 2016). Briefly, they were scraped gently using bladder and cultured in Advanced DMEM/F12 medium containing 10mM HEPES, 1XPenicillin-Streptomycin, 2 mM GlutaMAX, 1XN2 supplement, 50 ng/mL mEGF, and 1 mg/mL Rspodin for 12 h. After that, complementary medium was replaced with serum-free DMEM/F12 medium for 24 h and the conditioned medium was collected.

METHOD DETAILS

CAR T cells: Vector generation, T cell isolation, expansion, and CAR T cells generation

The second generation anti-MESO CAR lentiviral construct, which included mCherry reporter, CD8 hinge, meso scFv, 4-1BB and h28 signaling domains (described in (Milone et al., 2009)). was a gift from Michael C. Milone (University of Pennsylvania). For generation of the anti-Meso-Ch25h CAR plasmid, a cassette encoding a 54 nucleotide self-cleaving peptide (T2A) positioned 5' of *Ch25h* was commercially manufactured (Genscript, NJ) with 5' AvrII and 3' Sall restriction sites flanking the sequence and inserted into this vector as shown in Figure 7A. Similar strategy was employed to modify the anti-CD19 CAR retrovirus backbone consisting of a CD8 hinge, CD19 scFv, and 4-1BB domains (obtained from Andy J. Minn, University of Pennsylvania). The final constructs were verified using AvrII and Sall restriction digests and Sanger sequencing of the T2A-Ch25h insert using the final anti-MESO-Ch25h or anti-CD19-Ch25h constructs as the templates.

Mouse T cells or CD8⁺ T cells were isolated from spleen of different genetic mice with T cell or CD8⁺ T cell isolation kit. Human T cells were isolated from healthy male and female donors with age of 18–55 by the Human Immunology Core at the University of Pennsylvania and used for study immediately after isolation. T cells were stimulated with Dynabeads Mouse T-Activator CD3/CD28 beads or Dynabeads Human T-Activator CD3/CD28 beads for 48 h and were separated from beads prior to transduction. Indicated retroviruses were added into retronectin (20 μg/mL) pe-coated 24-well plate and spun down at 1000g for 1 h. Activated T cells were transduced with viruses at MOI = 3000 for 48 h. Transduction efficiency, expression of anti-MESO and anti-CD19 CARs and expression of *Ch25h* were assessed using flow cytometry and quantitative RT-PCR (qPCR) analysis, respectively.

Cytotoxicity, viability and exhaustion assays

OT-I-WT or *-Ch25h^{-/-}* splenocytes were *in vitro* stimulated with OVA peptide (0.5 μg/mL for 48 h) followed by treatment with vehicle or TDFs in the presence or absence of 25HC (4 μM) for 8 h. Then, these differentially treated-CTLs were co-cultured with target MC38OVA cells expressing luciferase at indicated E/T ratio for 4 h. For CAR T cells setting, anti-MESO or anti-CD19 CAR T cells were generated and treated with Vehicle or 25HC at 4 μM for 8 h. After that, CAR T cells were co-cultured with target EM-Meso-GFP-Luc or B16F10-hCD19-luc cells at indicated E/T ratio for 4 h followed by the luciferase-based cytotoxicity assay.

For the luciferase-based cytotoxicity assay (described in detail in (Zhang et al., 2022)), target cells alone were set as negative control with spontaneous death RLU and target cells lysed with water were set as positive control with maximal killing RLU. After 4 h co-culture, 100 μL of luciferase substrate (Promega Bright-Glo) was added to each well containing CTLs and target cells. After 10 min incubation, luminescence was measured using the EnVision (PerkinElmer) plate reader. The percentage of killing was calculated using the formula:

$$\% \text{ lysis} = 100 \times (\text{spontaneous death RLU} - \text{tested RLU}) / (\text{spontaneous death RLU} - \text{maximal killing RLU}).$$

For the viability and exhaustion assay, we co-cultured OT-I or CAR T CTLs with respective target cells for 2, 4, 8 or 16 h, washed with PBS and analyzed by flow cytometry using appropriate antibodies such as: anti-CD8-APC/Cy7, anti-CD69-PE, anti-PD-1-BV605, anti-LAG3-PE/Cy7, anti-CD366-BV421 and anti-Annexin V-FITC. Following staining, cells were washed with FACS buffer and mixed with counting beads followed by flow cytometry analysis.

Flow cytometry of tumors or spleens, immunofluorescence, immunoprecipitation and immunoblotting

For immunoprofiling of solid tumors, tumor tissue was dissected and digested with 1 mg/mL Collagenase D (Roche) plus with 100 μg/mL DNase I (Roche) in RPMI medium with 2% FBS for 1 h with continuous agitation at 37°C. Digestion mixture was passed through 100 μm cell strainer to prepare single cell suspension and washed with PBS supplemented with 2mM EDTA and 1% FBS. Single cells were stained with cell surface antibodies: anti-CD45-APC/Cy7, anti-CD3-PE, anti-CD8-AF700, anti-CD69-BV421, anti-PD-1-PE/Cy7, anti-LAG3-BV650, anti-CD336-BV421 and Annexin V-APC. Following staining, cells were washed with PBS and subjected to flow cytometry analysis.

For leukemia model, mouse blood was collected through retro-orbital bleeding and red cells were removed using RBC lysis buffer. After washes with PBS, cells were stained with anti-hCD19, anti-human CD19 CAR, anti-human CD8 on ice for 30 min. Following staining, cells were washed with PBS and subjected to flow cytometry analysis.

For spleen immune profile assay, spleens were ground up and passed through 40 μm cell strainer. Red cells were removed using RBC buffer. After that, single cells were incubated with anti-CD8-AF700, anti-CD4, anti-CD19, anti-NK1.1, anti-CD69, anti-PD-1 and anti-Annexin V antibodies.

For immunofluorescence analyses, the samples were prepared as previous described (Lu et al., 2021) and the Biotin anti-mouse CD3 antibody (1:100), Alexa Fluor 594 streptavidin antibody 1:500, Alexa Fluor 488 anti-mouse (1:100) were used as indicated.

For analysis of ATF3 sumoylation, OT-I WT T cells were isolated and stimulated with OVA peptide (0.5 μg/mL for 48 h) followed by treatment with Vehicle or TCM in the presence or absence of TAK981 (0.1 μM) for 12 h. Cells were lysed, and 1 mg of pre-cleared protein lysates from each sample were taken into immunoprecipitation using rabbit anti-mouse ATF3 antibody. Immunoprecipitation was carried out as previously described (Huangfu et al., 2012) and resulting precipitates were analyzed by immunoblot using primary antibodies against SUMO1 (3 μg/ml), ATF3 and secondary antibodies (VeriBlot for IP Detection Reagent HRP, 1:200), and goat anti-mouse HRP-conjugated antibody (1:5000). Loading levels in initial samples was controlled by direct immunoblot using antibody against β-tubulin (1:1000).

Flow cytometry analysis of trogocytosis

OT-I and CAR T settings were used to assess the extent of trogocytosis. In OT-I settings, splenocytes isolated from OT-I WT (*Ch25h^{+/+}*) or OT-I *Ch25h^{-/-}* mice were stimulated with OVA peptide (0.5 μg/mL for 48 hr) followed by treatment with Vehicle, IECM, PGE₂ (10nM), VEGF165 (50 ng/mL) or TCM in the presence or absence of 25HC (4 μM) or GW3965 (2 μM) for 8 h as indicated. For DiD labeling, MC38 or MC38OVA cells were stained with 0.3 μM DiD (1,1'-dioctadecyl-3,3,3',3'-tetramethylindodicarbocyanine) at 37°C for 10 min followed by PBS washes for 3 times. A total of 1x10⁵ treated-CTLs were co-cultured with DiD-labeled target cells in 96-well plates at a 5:1 of ratio for indicated times. After co-culture, cells were washed with PBS and stained with anti-CD8-APC/Cy7, PE-anti-mouse H-2K^b binds to SIINFEKL antibody on ice for 30 min. Following staining, cells were washed with FACS buffer and subjected to flow cytometry. Trogocytosis was tested by the acquisition of either DiD or OVA-MHC-I complexes by the CD8⁺ CTLs.

In CAR T cell setting, a total of 1x10⁵ CAR T cells were co-cultured with target cells at a 1:2 ratio for 4 h. After co-culture, cells were washed with PBS and stained with anti-CD8-APC/Cy7, anti-CD19 CAR and anti-hCD19 on the ice for 30 min. Following staining, cells were washed with FACS buffer and subjected to flow cytometry. Trogocytosis was tested by the acquisition of either MESO or hCD19 antigens by the CAR T cells and the loss of the CD19 antigen on target tumor cells.

For the inhibition of trogocytosis, CTLs or CAR T cells were pre-treated with vehicle of latrunculin A (1 μM) at 37°C for 20 min before co-incubation with target cells. In the Transwell setting, parental or DiD-labeled MC38 were seeded into the upper portion of Transwell chambers and T cells were seeded on the bottom these plates.

Quantitative real-time PCR

Total of RNA of CD8⁺ T cells which was treated with Vehicle or TCM or isolated from tumor tissue was extracted using RNA isolation kit. Concentration of RNA was measured by nanodrop2000 and the mRNA expression of *Ch25h* and *Atf3* were tested using real-time PCR. Primer sequences are provided in [Table S1](#).

Chromatin immunoprecipitation (ChIP) analysis

OT-I WT T cells were isolated from spleen of OT-I WT mice and stimulated with OVA (0.5 μg/ml) for 48 h followed by treated with FCM or TCM for 12h. T cells were harvested and the Immunoprecipitation (IP) was conducted following instruction from SimpleChIP Plus Enzymatic Chromatin IP Kit. ATF3 antibody used for the IP was Rabbit anti-mouse ATF3 antibody (1:50). The ChIP-qPCR for the *Ch25h* promoter used the following primers: forward 5-TAGCAGCCCATGCTGAGACTATGT-3' and reverse primer, 5 TTCTTTAG-CAGGGAAAGGGAGGTG-3'.

Tumorigenesis studies

For syngeneic subcutaneous tumor model, B16F10 (1x10⁶), MC38 (1x10⁶), MH6499c4 (1x10⁶) and Hepa1-6 (2x10⁶) were s.c inoculated into right flank of mice and tumor size was measured every other day using caliper. Tumor volume was calculated as width x width x length x 0.5 and mice survival were tracked until tumor volume reached ~1000 mm³.

Combination therapy and CAR T therapies

For the therapeutic combination of TAK981 with PD-1, MC38 (1x10⁶) cells were suspended into 100 μL PBS and inoculated into the right flank of *Ch25h*^{+/+} and *Ch25h*^{ΔCD8} mice at day 0. TAK981 was dissolved in 20% hydroxypropyl beta-cyclodextrin and formulated as previously described ([Lightcap et al., 2021](#)). Vehicle or anti-PD-1 (i.p, 5 mg/kg every 4 days) or TAK981 (i.v, 15 mg/kg, twice a week) or combination were injected into tumor-bearing mice when the tumor volume reached ~50-80 mm³. Tumor tissues were collected at day 25 for immune profiling analysis. For the mice survival analysis, mice were euthanized when tumor volume reached.

For anti-MESO/anti-MESO-Ch25h CAR T therapy, human EM-Meso-GFP-Luc cells (s.c., 1x10⁶) were inoculated into the right flank of NSG mice at day 0. Human anti-MESO-CAR or anti-MESO-Ch25h CAR T cells (generated as described above) were i.v. injected into tumor bearing mice at dose of 1x10⁶/mouse at days 16, 23, 30 and 37; PBS was used as control. Tumor tissue was collected at day 45 for immune profiling. For the survival analysis, mice were euthanized when tumor volume reached ~1000 mm³.

For anti-CD19/anti-CD19-Ch25h CAR T therapy, B16F10-hCD19 cells (s.c, 0.3x10⁶) were inoculated into the right flank of *Rag1*^{-/-} mice at day 0. Mouse anti-CD19 CAR or anti-CD19-Ch25h CAR T cells were generated and i.v. injected into tumor bearing mice at dose of 2x10⁶/mouse at days 7 and 13. Tumor tissues were digested at day 19 for immune profiling analysis. For the survival analysis, mice were euthanized when tumor volume reached ~1000 mm³.

For CAR T therapy of acute lymphoblastic leukemia model, GFP⁺NALM6 cancer cells were inoculated into NSG mice (i.v, 1x10⁶) at day 0. Human anti-CD19 CAR or anti-CD19-Ch25h CAR T cells were injected (1x10⁶) into tumor bearing mice at day 10, and PBS injection was used as the control group. Peripheral blood was collected via retro-orbital bleeding at days 17, 24 and 31 and lymphocytes were used for flow cytometric analysis. For the survival analysis, mice were euthanized when became moribund.

TROGOCYTOSIS AND VIABILITY ASSAY IN VIVO

MC38 or MC38OVA cells were inoculated into the right flank of *Rag1*^{-/-} mice (1x10⁶, s.c). WT OT-I and *Ch25h*^{-/-} OT-I splenocytes were stimulated *in vitro* with OVA peptide (0.5 μg/ml for 48 h). After stimulation, *Ch25h*^{-/-} CTLs were stained with CFSE (1nM) at 37°C for 10 min followed by wash with PBS for 3 times. Following wash, WT CTLs (1x10⁶, CFSE negative) were mixed with CFSE-labeled *Ch25h*^{-/-} CTLs at a ratio of 1:1 and re-suspended in 50μL PBS. This cell mixture was injected into MC38 or MC38OVA tumors. Twenty-four hr after injection, tumor tissues were digested into single cell suspension; and percentage of CD8⁺CFSE⁺, CD8⁺CFSE⁻, OVA⁻MHCI⁺CFSE⁺ and OVA⁻MHCI⁺CFSE⁻ cells were analyzed using flow cytometry.

For analysis of effects of TAK981 on trogocytosis, 1x10⁶ MC38-OVA cells were injected (s.c) into right flank of *Rag1*^{-/-} mice. 13 days after tumor inoculation, tumor bearing mice received OT1 CD8⁺ T cells injection (2x10⁷/mouse, intratumorally) and TAK981 injection (15 mg/kg, i.v) simultaneously. 24 h after injection, tumor tissues were harvested and trogocytosis and T cells exhaustion were analyzed with flow cytometry.

RNA sequencing analysis

WT OT-I or *Ch25h*^{-/-} OT-I splenocytes were stimulated with OVA peptide (0.5 μg/mL for 48 h) followed by treatment with FCM or TCM for 8 h *in vitro*. Total RNA was extracted with RNeasy Plus Mini Kit (QIAGEN). These samples were then used for RNA sequencing carried out as previously described ([Amorim et al., 2019](#)). The adaptor-trimmed reads were aligned to the mouse genome mm10 by STAR v. 2.7.2days with default parameters. Expression levels for each gene were counted by VERSE v. 0.1.4. Normalization and differential expression (DE) analysis was conducted by DESeq2 v. 1.28.1 using Vehicle-treated group as the control. Significantly DE genes were defined as those with Bonferroni adjusted p-value < 0.01 and log₂ (fold change) > 0.58 or < -0.58. Pathway enrichment analysis involves the statistical identification of particular biological function/process categories that are overrepresented in the specified gene collection. Total DE or down-/up-regulated genes were submitted to the Kyoto Encyclopedia of Genes and Genomes, respectively. Significantly enriched pathways (p-value < 0.05) were determined through gene set enrichment analysis integrated in

the R/Bioconductor package cluster Profiler v. 3.14.3. Seven KEGG pathways ('00,100', '00,120', '00,900', '04,975', '04,976', '04,979', '05,417') were defined as the cholesterol related collection, of which p-values and fold changes were used for downstream heatmap plotting. Data have been submitted to Gene Expression Omnibus (GSE190702).

Metabolomics studies

WT OT-I⁺ or *Ch25h*^{-/-} splenocytes were stimulated with OVA peptide (0.5 μg/ml) for 48 h followed by treatment with vehicle or TCM for 8 h *in vitro*. These cells then were spun down at 250g for 5 min followed by wash with 1 mL PBS twice. After this, cell pellet was suspended in 1 mL of ice-cold (-48°C) 80% (v/v) methanol: water followed by centrifuge the solution at -9°C, 11,500 g for 10 min. Finally, cells pellets were frozen in liquid nitrogen for 30s and stored until analysis. Samples were extracted using a biphasic extraction (Tambellini et al., 2013) and then subjected to lipidomics analysis by spotting on a 24 well PTFE slide and analysis by desorption electrospray ionization (Takats et al., 2004), on a Waters Xevo G2-XS qtof instrument. Pixels from technical replicates were averaged and 8564 features were detected. A targeted analysis was performed for 25HC m/z 385.3465, representing the [M+H-H₂O]⁺ ion of hydroxysterols (DeBarber et al., 2008).

QUANTIFICATION AND STATISTICAL ANALYSIS

All experiment described here are the representative of at least three independent experiments ($n \geq 5$ mice for each group unless specifically indicated). For *in vitro* experiments, cells or tissues from each of these animals were processed (at least) in biological triplicates. All data here were shown as average \pm S.E.M. Statistical analysis between two groups was conducted with 2-tailed Student t test and multiple comparisons was performed by using One-way ANOVA or two-way ANOVA analysis with Tukey's multiple-comparison. Tumor growth curve analysis was conducted with Repeated-measure two-way ANOVA(mixed-model) with Tukey's multiple-comparison. The Kaplan-Meier curves were used to analyze the survival data, and Cox regression was used to compute hazard ratio. No methods were used to determine whether the data met assumptions of the statistical approach. All statistical analysis was performed using GraphPad Prism 9 and the results of statistical analyses for each experiment are clearly indicated in the respective figures and in the Figure Legends. p values <0.05 were considered significant.

Human databases analysis

We performed Kendall Correlation analysis between CD8A expression, which is used for measuring CD8⁺ T cell presence in the tumor microenvironment, and CH25H expression in human cancer tissues from GENT2. Weak positive association between CD8A and CH25H was generated using the ggpubr (ggpubr: 'ggplot2' Based Publication Ready Plots. R package version 0.4.0.) and ggplot2 (ggplot2: Elegant Graphics for Data Analysis. Springer-Verlag New York, 2016) packages in the graphical and statistical software R (R: A language and environment for statistical computing. R Foundation for Statistical Computing, Vienna, Austria). Timer 2.0 (Li et al., 2020) was used to analyze the correlation between immune cell infiltration and *Ch25h* expression in human melanoma. The expression of *Ch25h* in T cells was analyzed while controlling for age, gender, and disease stage. Those tumors that showed a survival benefit associated with increased *Ch25h* expression in T cells were then further analyzed for tumor purity and *Ch25h* expression.